Electron scattering from molecules and molecular aggregates of biological relevance

Jimena D. Gorfinkiel

School of Physical Sciences, The Open University, Walton Hall, Milton Keynes, United Kingdom

E-mail: Jimena.Gorfinkiel@open.ac.uk

Sylwia Ptasinska

Radiation Laboratory and Department of Physics, University of Notre Dame, Notre Dame, Indiana 46556, USA

E-mail: sptasins@nd.edu

Abstract.

In this Topical Review we survey the current state of the art in the study of low energy electron collisions with biologically relevant molecules and molecular clusters. We briefly describe the methods and techniques used in the investigation of these processes and summarise the results obtained so far for DNA constituents and their model compounds, amino acids, peptide and other biomolecules. The applications of the data obtained is briefly described as well as future required developments.

PACS numbers: 34.80.-i, 36.40.Qv, 87.14.ef, 87.14.gf, 87.53.-j

Keywords: Submitted to: *J. Phys. B: At. Mol. Phys.*

1. Introduction

One of the main challenges of the XXI century is to respond to the medical needs of a growing and ageing population. Over 20 million new cancers are predicted for 2030 (Ferlay et al. 2013). The improvement and development of current and new cancer treatments is therefore a major scientific concern. Radiation therapy, that is, the use of highly energetic, ionising radiation, is employed to treat around 50% of cancer patients (Baskar & Itahana 2017). Its relative low cost compared to other treatments makes it particularly appropriate for use in developing countries, where cancer-survival rates require improvement. In addition, radiation is also used for medical imaging and understanding of its interaction with biological material is important for radiation protection (not only on Earth but also during space missions).

The first medical use of radiation was in imaging (X-rays) and the treatment of skin conditions (UV light). By the 1930's protocols for the use of radiation to treat some cancers had been developed. These days, treatments are highly sophisticated, using several types of ionisation radiation (photons, alpha particles, ions, etc.) and a variety of methods to ensure dose is maximized for the cancer cells while protecting healthy tissue. Overall, radiotherapy developments have been based on experimental knowledge and empirical methods. Nowadays, however, efforts are being made to develop a deeper understanding of the underlying molecular processes in order to design models and software to aid these developments.

Any type of ionising radiation interacting with a medium will produce large number of secondary electrons, the product of enough energy being transferred between projectile and target to ionise the latter. Around 10^4 electrons with energies below 30 eV are generated per MeV of deposited radiation (Pimblott & LaVerne 2007, Alizadeh & Sanche 2012). The experiments of Boudaïffa et al. (2000) confirmed that subionisation electrons can produce single and double-strand breaks (SSBs and DSBs, respectively) in DNA via the process known as dissociative electron attachment (DEA). This work marked the beginning of intense experimental and theoretical interest in electron interactions with biologically relevant molecules, particularly DNA components, as well as DNA strands. The aim of this research is to provide an understanding of the mechanisms of electron induced damage, as well as quantitative data to be used in its modelling. A lot of the work has been performed in the gas phase (or, the computational equivalent, isolated molecules). Researchers recognise, however, that radiation damage in the cell occurs in a condensed medium and that the environment (fundamentally, the water that surrounds cell constituents) will modify the electron-molecule interaction and its outcome. For this reason, studies in the condensed phase (mostly films) and, more recently, in pure and hydrated clusters have been performed.

It should be pointed out that an understanding of radiation effects at the molecular level is only a small part of the knowledge needed to accurately describe (and predict) biological radiation damage. A number of other effects (dose deposition, repair mechanisms, indirect mechanisms like the bystander effect, etc.) contribute to the complex biological process and must be taken into account (Hall & Giaccia 2012). We should also mention that many exciting developments in the field of cancer treatment are currently taking place (from the concurrent use of radio and chemotherapy to genetics-based approaches) not all of which involve the use of radiation. It is the case however, that radiation will remain a highly used tool both for treatment and imaging.

The aim of this Topical Review is to provide an overview of the research performed so far on electron collisions with biological targets, summarising the main finds and how this information is relevant, both from an applied perspective and a fundamental one. A prior review (Baccarelli et al. 2011) described the work performed up to 2011, particularly on resonance formation and DEA. We also refer the reader to two recent reviews of DEA (Fabrikant et al. 2017) and DEA to biomolecules (Bald et al. 2017) for more details regarding this process. In this Topical Review, we will concentrate on

more recent work and include all electron-induced processes as well as widen the range of targets including aggregates. Results from aggregates can bridge our understanding of electron-induced processes in the gas and condensed biomolecules, including DNA and its constituents. A comparison of results from different states of matter has already revealed the basics mechanisms initiated by electron scattering and how they are modified under conditions more related to those in the cell (Alizadeh & Sanche 2012). These mechanisms can assist in a better interpretation of the role of secondary electrons in radiation-induced damage as well as in potential applications to radiotherapy (Sanche 2016). We will also describe some electron-biomolecule interactions not related to biological radiation damage.

1.1. Targets and processes of interest

The work described in this Topical Review corresponds to low-energy collisions. We define these as collisions happening below ≈20 eV (i.e., not much above the ionisation threshold). Low energy electrons (LEEs) can scatter elastically or lead to the excitation (rotational, vibrational and/or electronic) of the target molecule. This excitation can lead to (neutral) dissociation. In addition, DEA can take place. This is a resonant process that involves electron capture by a molecule, AB, to produce a temporary molecular anion (also called a transient negative ion, TNI, or resonance), $(AB)^{*-}$ that can then dissociate into an anion, A^-, and a neutral radical or radicals, B·, according to the following reaction:

$$e^- + AB \longrightarrow (AB)^{*-} \longrightarrow A^- + B\cdot$$

where A^- and B· are atoms and/or molecular fragments. DEA can lead to both simple, single bond cleavage or a more complex decomposition into a number of fragments; it is also extremely effective at selectively breaking specific molecular bonds. The experiments of Boudaïffa et al. (2000) demonstrated clearly the presence of resonant features in the occurrence of SSBs and DSBs as a function of electron kinetic energy; that is, they showed that DEA played a major role in DNA damage.

Resonances are classified according to whether they involve fundamentally the electronic states of the target or they involve nuclear (vibrational) degrees of freedom. The electronic resonances are classified into shape, when the electron attaches to the molecule in its ground state (the ground state is then described as the parent state of the resonance) and core-excited, when the electron attaches to the molecule an electronic excited state (Schulz 1973*a*, Schulz 1973*b*). In shape resonances the incoming electron is trapped by the potential resulting from a combination of short-range attractive and long-range repulsive forces (the latter are caused by the angular-momentum barrier of the incoming electron). These resonances can be seen as the incoming electron being trapped in one of the unoccupied orbitals of the molecule. In core-excited resonances the incoming electron can be seen as electronically exciting the target molecule to a

state (the parent state) and then being trapped into one of the empty spin-orbitals. Core-excited resonances are further classified as Feshbach (also known as Type I) or core-excited-shape (known as Type II) . In the latter the resonance is energetically above its parent state and can therefore decay (via autoionisation) to it and in the former it lies below (Herbert 2015)‡. Feshbach resonances have lifetimes much larger than shape or core-excited shape resonances and, consequently, very narrow widths. Vibrational Feshbach resonances (VFR) involve nuclear motion and usually occur at very low energies when the electron is trapped into a diffuse (dipole-bound) state and its energy transferred to the molecular vibrations (since the anion state is weakly bound, it tends to lie slightly below the ground state of the neutral target and therefore its vibrational levels are very close, but slightly below the corresponding vibrational states of the neutral target). VFRs are likely to occur in molecules with large polarizability and/or a very large dipole moment that leads to a long-range attractive interaction (large dipole moments can also lead to the very-low energy formation of scattering-type dipole states that might lead to anion stabilization as an alternative route to DEA (Carelli & Gianturco 2016)). VFRs are found just below the thresholds for vibrational excitation of the target molecule.

At higher energies (≈10 eV for most of the molecules discussed here) ionisation becomes energetically possible and so does ion pair formation/dipolar dissociation. Data (cross sections) for a broad energy range are needed for the description of radiation interaction with matter, for example using Monte Carlo-based techniques. In addition, the computational description of DEA requires information on the temporary anions formed (energy and lifetime). In this Topical Review, we will summarise work available on most of the relevant low-energy cross sections (neutral dissociation and rotational excitation are excluded because of the very little available data) as well as theoretical work on resonance characteristics.

In principle, all biological molecules present in the cell are of potential relevance to understanding the effects of radiation. In addition, electron scattering data for some inorganic molecules is also highly relevant. The most significant of all is water, the main constituent of most living organisms. Other molecules used in track structure modelling (see Section 5.1.1 for more details) are N_2, CH_4 and CO_2 (these are employed to produce tissue equivalent gas). We will not review work on these inorganic targets here, so we refer the reader to earlier reviews: Itikawa & Mason (2005) for water, Anzai et al. (2012) for water and CO_2, etc..

DNA (and RNA) constituents have been the focus of a lot of the experimental work: not only the bases and sugar, but also nucleosides and nucleotides as well as as short DNA strands. Collisions with substituted DNA bases (in particular halo-substituted) have been studied as these substitutions can render the molecules more prone to radiation-induced break-up, in other words, these molecules have the potential

‡ We note that this classification is somewhat over-simplifying: resonances that have a mixed shape and core-excited character have been identified (e.g. Nenner & Schulz 1975, Winstead & McKoy 2007) as well as other resonances that have more than one parent state.

to act as radiosensitisers, enhancing the effect of radiation on the DNA. Similarly, the effect of electrons colliding with cisplatin, a chemotherapy drug, has also been studied.

Other cell constituents, in particular amino acids and peptides, have been investigated. In addition, researchers have also looked at targets that can be considered models for the biologically relevant molecules. The choice of these simpler systems was dictated by the fact that they require less computational effort and/or are easier to study experimentally. Targets of these type are, for example, tetrahydrofuran (THF) a five-membered heterocyclic compound which may be considered a hydrogenated form of furan and is regarded as the elementary prototype of deoxyribose, and pyrimidine. In this Topical Review, we will refer to work performed on these targets only when it provides insight not yet available for the 'true' biological targets. We also briefly mention other types of biological targets whose interaction with LEEs has been investigated. These include other radiosensitisers, molecules involved in biological electron transfer, etc.

1.1.1. Types of cross sections Cross sections can be classified in many different ways. We will summarize here the type of cross sections that are discussed in this Topical Review. Cross sections can be presented as an integrated (over all parameters) quantity or as differential cross sections. The former depend on the scattering energy only and are normally referred to as integral cross sections. The latter, in the energy range of interest to this Topical Review, are normally angular differential cross section that are provided for a specific scattering energy as a function of the scattering angle (these cross sections can also be provided for a specific scattering angle as a function of scattering energy; these are normally referred to as excitation functions).

Cross sections can either be determined for a specific process or for a sum of these. A total cross section (TCS) quantifies the probability that all scattering process take place. These cross sections can be measured with (relative) ease. Elastic cross sections quantify the probability that the electron interacts with the target but does not modify its internal state. We note that in experimental measurements it is impossible to measure fully elastic cross sections: due to limitations in the detectors, etc., these cross section normally include some rotational excitation (Sanz et al. 2014). In *ab initio* calculations, the motion of the nuclei is normally ignored but the use of Born-type approximations for polar molecules (see later) means that the elastic cross sections normally implicitly include excitation from the lowest rotational state of the target to a handful of excited states (see Section 2.1).

Momentum transfer cross sections are not usually published, although their determination from elastic differential cross sections is straightforward, and less problematic than for the integral elastic cross section (because the integration over scattering angle involves a $(1 - \cos$ term), instead of sin, making the small angles contribution irrelevant).

Vibration and electron excitation cross sections can be measured and calculated: it is not always possible, however, to provide state-to-state experimental results so cross

sections are regularly provided for excitation to a group of states.

Finally, DEA cross sections can also be determined both experimentally and theoretically (the latter, only for processes involving a very reduced number of degrees of freedom). However, it is much more usual for experimental work to provide ion yields as a function of scattering energy, given the difficulty in turning these into absolute values and thus cross sections. Additionally, instead of the absolute cross section, ion yields can be represented as a cross section relative to a well known resonant cross section, for example, that describing Cl^- production from CCl_4 at 0 eV. The Cl^- yield at a given CCl_4 pressure, electron current, etc. is measured and then the same conditions are used to perform measurements for the molecule of interest. By comparing ion yields and using the known value of the cross section for Cl^- production from CCl_4, the cross section for the production of a fragment from the molecule of interest is deduced. In this way, relative DEA cross sections are determined.

1.2. Acronyms

CC: close-coupling
DCS: elastic (angular) differential cross section
DEA: dissociative electron attachment
DSBs: double stand breaks
ECS: integral elastic cross section
EELS: electron energy loss spectroscopy
ESD: Electron stimulated desorption
ETS: electron transmission spectroscopy
LEEs: low energy electrons
MAC: magnetic angle changer
SE: static-exchange
SEP: static-exchange plus polarization
SSBs: single strand breaks
SMC: Schwinger multi-channel
SMCPP: Schwinger multichannel with pseudopotentials
TCS: total cross section
THF: tetrahydrofuran
TICS: total (summed over final states) electronic inelastic cross section
TNI: temporary negative ion

2. Isolated targets: methods

As already mentioned, most of the work done so far on electron collisions with biologically relevant targets has involved gas-phase molecules (and the corresponding theoretical equivalent, single isolated molecules). These studies can provide a level of

detail and understanding that collisions with more complex targets cannot: theoretical calculations are generally more accurate due to their reduced size and complexity. Experimentally, for example, the increased number dissociation pathways and the difficulty in detecting some of the products of DEA makes it hard to interpret anion spectroscopy data for condensed targets.

In this section, we review briefly the computational and experimental techniques most often applied to the study of electron scattering from biologically relevant targets.

2.1. Computational methods

The methods applied to biologically relevant targets are standard scattering methods, developed to treat general electron collisions with any molecular target (Huo & Gianturco 1995). The focus will be on those techniques that address the electronic part of the problem and the methods will be introduced within the Fixed-Nuclei Approximation (FNA). In this approximation, the nuclei in the molecule are treated as fixed in space during the collision. In Section 3.4.2, we will briefly discuss how nuclear motion is reintroduced to determine DEA cross sections. Below, we describe those low energy methods that have been applied most to biologically relevant molecules. Other low-energy techniques (i.e., the Complex Kohn variational method (Gianturco et al. 1995) that was applied to THF and the R-matrix eigenchannel method used to look at resonances in nucleobases (Tonzani & Greene 2006)) are not described. Similarly, a number of high energy methods exist for the determination of ionisation and other cross sections at high energies (e.g., IAM-SCAR/IAM-SCARD (Blanco & García 2002, Blanco & García 2003), the most widely used on biological molecules, the binary-encounter-Bethe (BEB) method, Deutsch-Mark Formalism) that can provide reasonable data for lower energies but will not be discussed either.

There are three sources of uncertainty in low-energy calculations of electron-molecule collisions: the description of the (non-interacting target (i.e. the model that is used to describe its internal states), the approximation used to describe the scattering processes (e.g. how the continuum is modelled, whether polarization is included) and the theoretical method (and the computational implementation) used to perform the scattering calculations. In the brief description below, we attempt to indicate how these affect each of the techniques. We note that the inclusion of polarization effects is crucial for the description of resonances (particularly of shape character): if these are not included (or are partially so) the resonance positions tend to be overestimated (Mašín & Gorfinkiel 2011). This incorrect position of the resonance will affect the size and behaviour of the cross sections. The effect can be particularly significant for electronic excitation cross sections if shape resonances are above the excitation threshold (da Costa et al. 2008*a*, da Costa et al. 2008*b*).

All methods described below are based on the partial-wave expansion of the continuum wavefunction. In general, only a few partial wave are included in these calculation. As we will see later (Section 3.1), when the target molecules have a

permanent dipole moment, it is necessary to include additional partial waves using less accurate methods.

In what follows, E denotes the kinetic energy of the scattering electron, Y_{lm} a spherical harmonic corresponding to angular momentum l and its projection m and $\mathcal{A}$ is the antisymmetrization operator; H is the total Hamiltonian for the target + scattering electron system, and H^N is the N-electron target Hamiltonian. Finally, Γ indicates the irreducible representation a function belongs to.

2.1.1. Schwinger multichannel method This method has been applied to biologically relevant molecules by a number of researchers in Brazil and the U.S.A.. A more detailed description can be found in da Costa, Varella, Bettega & Lima (2015). This variational approach is based on the Lippmann-Schwinger integral equation (Takatsuka & McKoy 1984). In it, the scattering amplitude is determined from the following equation:

$$f(\mathbf{k}_f, \mathbf{k}_i) = -\frac{1}{2\pi} \sum_{nm} \langle S(\mathbf{k}_f)|V|\chi_n\rangle (d^{-1})_{nm} \langle \chi_m|V|S(\mathbf{k}_i)\rangle \tag{1}$$

where $\mathbf{k}_{i,f}$ are, respectively, the initial and final wave-number, V is the electron molecule scattering potential (comprising the electrostatic repulsion/attraction of the scattering electron by the electrons and nuclei of the target respectively) and the $S(\mathbf{k}_i)$ describes an asymptotic state, solution of H_0, the non-interacting Hamiltonian (sum of H^N and the kinetic energy operator for the scattering electron; the total Hamiltonian for the system is therefore $H = H_0 + V$). Also,

$$d_{nm} = \langle \chi_n|A^+|\chi_m\rangle \tag{2}$$

with the functions χ_n forming some trial basis and:

$$A^+ = \frac{\hat{H}}{N+1} - \frac{\hat{H}P + P\hat{H}}{2} + \frac{VP + PV}{2} - VG_P^+V \tag{3}$$

where $\hat{H} = (E - H)$ and G_P^+ is the free particle Green's operator projected onto the P space of the energetically open electronic states of the target molecule:

$$G_P^+ = PG_0^+ \quad \text{and} \quad G_0^+ = \lim_{\eta\to 0} \frac{1}{E - H_0 + i\eta} \, . \tag{4}$$

In general, $\chi_m = \mathcal{A}\Phi_n\psi_j$ where Φ_n are eigenfunctions of H^N and ψ_j are single-particle functions.

The relevant scattering quantities (cross sections, resonance positions) are obtained from the $f(\mathbf{k}_f, \mathbf{k}_i)$. Two implementations of the method are regularly used to study electron-molecule scattering: the one developed in Caltech and the Brazil one (SMCPP method) that makes use of norm-conserving pseudopotentials to describe the core electrons. Most calculations are performed within the Static Exchange (SE) and Static Exchange plus Polarization (SEP) approximations using, for Φ_n, a single determinant description of the ground electronic state of the target molecule. The

single particle wavefunctions (bound and scattering orbitals) are normally expanded in a basis of Gaussian-type orbitals (GTOs). When excited states are included, a configuration interaction (CI) singles approximation§ is used to describe them (da Costa et al. 2005). The computational effort required, however, means that no calculations including excited states have been performed for the type of molecules included in this Topical Review. Both SMC (Winstead & McKoy 1996) and SMCPP (dos Santos et al. 2012, da Costa, Varella, Bettega & Lima 2015) implementations are parallelized. The use of pseudopotentials confers this method a great advantage when treating targets involving heavy ions and/or large (electron rich) targets. This has enabled the SMCPP approach to be applied to halogen and sulphur containing targets. The method has been applied mostly to the determination of ECS and DCS as well as shape resonance energies of a variety of DNA constituents, some amino acids, radiosensitisers and model molecules.

2.1.2. R-matrix method The R-matrix method has been applied in the UK to a number of biologically relevant targets. A detailed description of it can be found in Tennyson (2010) (for electron-molecule scattering) and Burke (2011) (more generally). The basic idea of this method is to solve the problem by splitting space in two regions separated by a sphere of radius a. When the electron is close to the target, exchange and correlation effects are taken into account. When the electron is far from the target, the projectile-target interaction can be modelled in terms of a multipolar potential and the resulting equations are much easier to solve. Combining the solutions in these two regions allows the efficient determination of scattering data.

In the inner region, the wavefunction describing the collision is expressed in terms of the energy-independent R-matrix basis functions $\Psi_k(\mathbf{r}_1, ...\mathbf{r}_{N+1})$. These are expanded in the following way:

$$\Psi_k^\Gamma(\mathbf{r}_1, \mathbf{r}_2 \dots \mathbf{r}_{N+1}) = \mathcal{A} \sum_n^{n_c} \sum_j a_{njk} \Phi_n(\mathbf{r}_1 \dots \mathbf{r}_N) u_{nj}(\mathbf{r}_{N+1}) + \sum_i b_{ik} \chi_i(\mathbf{r}_1, \mathbf{r}_2 \dots \mathbf{r}_{N+1}) \; . \tag{5}$$

Here $\mathbf{r}_i$ describes the coordinates of the i^{th} electron, u_{nj} are (discretized) 'continuum' orbitals describing the scattering electron and Φ_n are usually multiconfigurational solutions of H^N describing electronic states of the target molecule with energy ε_n. χ_i are multi-centre quadratically integrable functions used to represent short range correlation and polarisation effects. The Ψ_k^Γ are eigenfunctions of the operator $H + L$ in the inner region with eigenvalues E_k (L denotes the Bloch operator, see Burke 2011). The coefficients a_{njk} and b_{ik} are obtained diagonalizing the matrix representing this operator

§ Any Quantum or Computational Chemistry coursebook will provide an introduction to this and other standard techniques for bound electronic structure calculations, for example Jensen (1999)

in the basis of $\Phi_n u_{nj}$ and χ_i. Molecular orbitals obtained from quantum chemistry codes are used to expand Φ_n and χ_i. A basis of GTOs is also used for u_{nj}.

A crucial point in applying this method is to determine what value the radius a should take: the electronic density associated to the target wavefunctions Φ_n must be negligible outside the R-matrix sphere. Using the Ψ_k^Γ, we can build the R-matrix at the boundary between regions‖:

$$R_{ij}(E) = \frac{1}{2a}\sum_k \frac{f_{ik}(a)f_{kj}(a)}{E_k - E} \quad \text{with} \quad f_{ik}(a) = \left\langle \frac{(\Phi_n)_i Y_{l_i m_i}}{r_{N+1}} \middle| \Psi_k^\Gamma \right\rangle_{inner} \tag{6}$$

where r_{N+1} indicates the radial coordinate of the scattering electron.

The wave function describing the collision has a simpler form in the outer region:

$$\Psi_k(\mathbf{r}_1, \mathbf{r}_2 \ldots \mathbf{r}_{N+1}) = \sum_i^{n_c}\sum_j \Phi_i(\mathbf{r}_1 \ldots \mathbf{r}_N)\frac{F_j(r_{N+1})}{r_{N+1}} Y_{l_j m_j}(\hat{\mathbf{r}}_{N+1}) \tag{7}$$

where n_c is the number of target states included in expansion (5) and $\hat{\mathbf{r}}_{N+1}$ indicates the angular coordinates of the scattering electron. $F_j(r_{N+1})$ are solutions of the following set of differential equations:

$$\left(-\frac{1}{2}\frac{d^2}{dr_{N+1}^2} + \frac{l_i(l_i+1)}{2r_{N+1}^2}\right) F_i(r_{N+1}) + \sum_{j=1}^{n} V_{ij}(r_{N+1})F_j(r_{N+1}) = (E - \varepsilon_i)F_i(r_{N+1}) \tag{8}$$

V_{ij} are coupling potentials describing the electron-target interaction (usually expanded in terms of the target electronic permanent and transition dipole and quadrupole moments, see Tennyson 2010). The set of Equations (8) are solved employing a propagation method (Burke 2011) and using boundary conditions calculated from the R-matrix (equation 6). The asymptotic form of the radial functions F_j is known and relates them to the K-matrix. Once the K-matrices are calculated, all relevant scattering data can be obtained.

This method has been used both at SE, SEP and close-coupling (CC) levels to calculate both elastic an electronic excitation cross sections as well as resonance parameters for shape and core-excited resonances. The quality of the calculations is dependent on the wavefunctions used to describe the electronic states of the target. Limitations in terms of the radius a mean diffuse states cannot be well described¶; limitations in the size of Hamiltonian matrix that can be diagonalized affect the description of excited states (i.e. the size of the active space used). In addition, polarization is whole (SEP model) or partially (CC calculations) included in the inner region (polarization effects are not normally described in the outer region) via

‖ The subscript *inner* indicates that the integration implied by the brackets is performed over the inner region.

¶ It is the use of GTOs to describe the scattering electron that makes it extremely difficult to use $a \geq 18$ a_0; however, a very recent implementation of the method, the UKRmol+ suite, that allows both for higher precision calculation and the use of B-splines to describe the continuum, has made it possible to use bigger radii.

the functions χ_i, whose form is dictated by the model used to describe the target (Tennyson 2010): the current implementation does not allow for active control over the amount of polarizability described (the SMC/SMCPP calculations also include additional configurations in their χ_n basis to describe polarization but the choice of these significantly reduced the problems associated to it). One big advantage of the method is that the computationally demanding part of the problem (the inner region) is independent of the scattering energy and therefore solved only once. This makes it 'cheap' to calculate cross sections, etc. for a large number of energies, making it easier, for example, to detect and characterize narrow resonances.

2.1.3. Single-centre expansion The single-centre expansion approach has been used mainly by the group of Prof. Gianturco in Rome. Further details of the theory can be found elsewhere (Gianturco et al. 1995, Gianturco & Jain 1986). The method is implemented in a software suite called ePolyScat (Gianturco et al. 1994).

In this approach, the electron-molecule interaction potential is built as a sum of three terms: a static contribution, an exchange contribution (that can be local or non-local depending on the target) and a correlation-polarization contribution that describes the response of the target electrons to the scattering one. This method, therefore, employs a one-electron picture of the scattering problem for the whole space (whereas the SCM method use an all electron description and R-matrix technique an all electron description in the inner region and a one-electron one in the outer region). The quality of the calculation therefore depends as much on the form of the potential terms as on the input (basis set, etc.) used to generate the wavefunctions.

This method is used at SE and SEP levels so only the ground electronic state of the target is considered and its wavefunction described by a single determinant (normally using Hartree-Fock orbitals). All single-particle wavefunctions are expanded around the centre of mass of the molecule, using a set of symmetry-adapted angular functions, $X_{lh}(\hat{\mathbf{r}}_i)$, given by the appropriate combination of spherical harmonics $Y_{lm}(\hat{\mathbf{r}}_i)$. For the molecular orbitals, the expansion is obtained by fitting multicentric orbitals calculated using standard quantum chemistry codes. For the wavefunction describing the scattering electron we have:

$$F^{\Gamma}(\mathbf{r}_{N+1}) = r^{-1} \sum_{l,h} f^{\Gamma}_{lh}(r_{N+1}) X_{lh}(\hat{\mathbf{r}}_{N+1}) \tag{9}$$

where $\hat{\mathbf{r}}_{N+1}$ is the angular coordinate of the scattering electron. The radial functions $f^{\Gamma}_{lh}(r_{N+1})$ are represented on a numerical grid. Assuming local interactions between the scattering electron and those of the target, $f^{\Gamma}_{lh}(r_{N+1})$ are solutions of:

$$\left[\frac{d^2}{dr^2} - \frac{l_i(l_i+1)}{r^2_{N+1}} + 2k\right] f^{\Gamma}_{(lh)_i}(r_{N+1}) = \sum_j V^{\Gamma}_{ij}(r_{N+1}) f^{\Gamma}_{(lh)_j}(r_{N+1}) \tag{10}$$

where $k = 2\sqrt{E}$. As stated, the physics of the problem is contained in the elements of

the coupling potential:

$$V_{ij}^{\Gamma}(r_{N+1}) = \int d\hat{\mathbf{r}} X_{(lh)_i}(\hat{\mathbf{r}}_{N+1}) V(\mathbf{r}_{N+1}) X_{(lh)_j}(\hat{\mathbf{r}}_{N+1}) \tag{11}$$

more specifically, in the form that $V(\mathbf{r}_{N+1})$, the interaction potential between the target and projectile, takes. In general, the exchange interaction is described by a local but energy dependent potential suggested by Hara and the short range correlation and (long range) polarization through another local (but energy independent) potential (for more details see, for example, Baccarelli et al. 2011). The set of coupled differential equations (10) are integrated numerically up to a maximum radius; a maximum value of l must be chosen for f_{lh}^{Γ}, the $X_{l'h}$ and the expansion of $V_{ij}^{\Gamma}(r_{N+1})$. The scattering information is obtained from the radial functions. Again, method is more easily applicable to larger target molecules than the R-matrix technique as the work described below demonstrates.

This technique has been used mainly to investigate resonance formation and determine ECS and DCS. The most recent implementation of the method is the program VOLSCAT (Sanna et al. 2009), so far used mainly for positron-biomolecule scattering.

2.2. Experimental methods

Below we describe the experimental techniques most usually applied to the study of electron scattering from biological molecules. We note that many of the biomolecules of interest are powder at room temperature and that this entails additional experimental difficulties (some of which are discussed below) and make it particularly difficult to provide absolute experimental cross sections.

2.2.1. Electron Transmission Spectroscopy One of the earliest experimental techniques used to study electron scattering from gas-phase targets is Electron Transmission Spectroscopy (ETS). This technique is used to investigate states of TNIs formed when a free electron with a specific energy is attached to normally unoccupied orbitals (Schulz 1973*a*, Modelli et al. 1982). Thus, ETS is suitable for the detection of short-lived anions formed in the equilibrium geometry of the neutral molecule since electron attachment happens at much shorter timescales than nuclear motion of the target. In this technique the total scattering cross section is obtained by measuring the unscattered electron current transmitted through a collision chamber filled with a gas. In general, electrons are emitted from a filament and their energy selected by a monochromator. The monochromatic electron beam passes through the collision chamber and then is retarded by a potential barrier produced by an electrode in front of the collector, which detects directly the derivative of the transmitted current. Thus, various vertical electron attachment energies of gas-phase molecules can be obtained, which can be related to resonance energies as well as the energies of the unfilled, positive energy, orbitals (negative electron affinity).

ETS was developed in late 60s and was mainly used to study electron collisions with atoms, diatomic, and even some polyatomic molecules. However, the instrumentation used at the time suffered many technical drawbacks (Allan 2012), such as low signal-to-noise ratio, non-linearity of electrodes potential versus electron energy and limited electron energy and angular ranges. Therefore, there was still limited data related to absolute cross sections for all processes (elastic, vibrational and electronic excitation, and DEA). Later on, this technique was significantly improved in order to measure small cross sections for high vibrational levels or for electronic excitation. For example, implementation of a magnetically collimated spectrometer with trochoidal analysers allowed for much higher sensitivity; the invention of the magnetic angle changer (MAC) allowed for more precise measurements of absolute cross sections and angular distributions (Read & Channing 1996, Zubek et al. 1996). Moreover, addition of mass spectrometers also benefited in expanding the capability of the existing ETS apparatus to study DEA processes.

Regarding electron scattering from molecules of biological relevance, the ETS technique was successfully employed to measure the derivative of a transmitted current through DNA bases (Aflatooni et al. 1998) and their model molecules, e.g., diazines (Nenner & Schulz 1975), other DNA constituents (Aflatooni et al. 2006), the RNA base uracil and its derivatives (Scheer et al. 2004) and selected amino acids (Scheer et al. 2007). All of these studies determined π^* anion state energies and vertical attachment energies for these compounds. In the last decade, TNI states formed in other biologically relevant molecules have been explored using ETS techniques, including trimethyl phosphate and several compounds containing the P=O group (Burrow et al. 2008). The range of investigated gas-phase targets has expanded to other cellular-related components, including naphthoquinone (Asfandiarov et al. 2014), indole (Modelli et al. 2013), plant hormones (Pshenichnyuk & Modelli 2014), antipyretics (aspirin, paracetamol, phenacetin, and ibuprofen) (Pshenichnyuk & Modelli 2012), the anti-malarial drug artemisinin and its derivatives (Modelli & Galasso 2007, Galasso et al. 2007) and flavonoids (Modelli & Pshenichnyuk 2013), as well as analogues of radiosenistizers (Modelli et al. 2011).

2.2.2. Electron Energy Loss Spectroscopy (EELS) An electron spectrometer for EELS consists of two identical hemispherical monochromators in tandem: a source of incident electrons and an analyser of scattered electrons, very often coupled with a MAC (Read & Channing 1996, Zubek et al. 1996, Linert & Zubek 2006, Allan et al. 2016). In general, similar to ETS, an electron gun produces an electron beam which is focused on the entrance of a double hemispherical deflector. Electrons exit the hemispherical deflector having a narrow energy distribution and are accelerated and then focused on a molecular-gas beam. Electrons scattered at a given angle are decelerated to a potential of the analyser and focused on the entrance aperture of the double hemispherical deflector. Afterwards, a set of electrostatic lenses placed behind the exit aperture of the analyser focuses transmitted electrons on a detector. The electron analyser can be rotated around

the molecular beam axis over an angular range from $-90°$ to $90°$ with respect to the direction of the incident electron beam. Such an arrangement allows the study of electron scattering in the angular range from $0°$ to $90°$ even without using the MAC.

Depending on the mode of operation, such instruments can be used to record three types of spectra: the energy-loss spectrum, the excitation function, and the angular distribution. In the case of energy-loss spectra, the scattered electron intensity is plotted as a function of the electron energy loss for a given incident electron energy. Such spectra indicate the presence of excited states of the target molecule, often including those accessible through spin and dipole forbidden transitions. The decay of these short lived metastable anions via autodetachment gives rise to vibrational excitation. Therefore, the various peaks detected in the energy loss obtained at the electron energy of a temporary anion, provide evidence of vibrational states in the low energy range (Abouaf et al. 2008).

In the case of the excitation functions, a signal is plotted as a function of the incident electron energy for a given energy loss. This approach is therefore used to obtain the energy and intensity of molecular transitions to excited electronic states. Similarly to ETS, such spectra indicate negative ion states; however, EELS is more versatile. Recent developments of this technique increased information about cellular components from 'fine structure' originated from excitation of vibrational molecular energy levels (Aronova & Leapman 2012).

Excitation of electronic states and resonant vibrational excitation were widely investigated in gas-phase biomolecules using EELS. For example, electron-impact excitation was studied for glycine (Abouaf 2008, Burean et al. 2008) and alanine (Abouaf 2008), cytosine (Abouaf et al. 2004), thymine (Abouaf & Dunet 2005, Bellert et al. 2003, Chernyshova et al. 2013), uracil (Abouaf & Dunet 2005, Chernyshova et al. 2012), and halouracil (Abouaf & Dunet 2005, Bellert et al. 2003), 5-nitrouracil (Abouaf et al. 2008), pyridine (Linert & Zubek 2016), pyrimidine (Regeta, Allan, Mašín & Gorfinkiel 2016, Regeta, Allan, Winstead, McKoy, Mašín & Gorfinkiel 2016, Linert & Zubek 2015) and THF (Zubek et al. 2011, Do et al. 2015) as well as even smaller model systems, such as acetoacetic acid, and in order to investigate the fundamental chemical and physical aspects of (excess) electron-induced proton transfer that can occur in biological systems (Keolopile et al. 2015).

Recently, due to improvements in the quality of the spectra obtained from EELS, two-dimensional (2D) electron energy loss spectra have also been reported for molecules that can serve as a simple model compound for nucleobases like pyrazine (Allan et al. 2016); systematic experiments for a series of molecules have been performed. The 2D spectra provide both state-to-state information and insight into the dynamics of nuclear motion in resonances: information about the motion of a nuclear wave packet on a resonant potential surface is possible since this wave packet (of the resonant state) follows one of two competing pathways: molecular dissociation (DEA) or electron detachment. If the electron is ejected, its kinetic energy is a measurable quantity and thus the spectra of the detached electron provide information about the mode and state

into which the wave packet propagated, and whether it changed modes by intramolecular vibrational energy redistribution. By changing the incident electron energy a specific vibrational state can be selectively populated and the motion of the wave packet along the path of the neutral molecule into the final vibrational state can be tracked. This technique of 2D spectra is a general tool for investigating nuclear dynamics of transient negative ions, and in the past it was used to study simple gas-phase molecules such as N_2 and CO_2 (Allan et al. 2016).

2.2.3. Dissociative Electron Spectroscopy In general, DEA studies are carried out using a crossed electron-molecular beam experiment. An effusive molecular beam containing biomolecules can be produced by: i) thermally heating a powder sample loaded to an oven with an attached capillary directed towards the reaction zone; ii) directly introducing a liquid sample with sufficient vapour pressure into the reaction zone. Since most biomolecules (e.g., nucleobases, amino acids, and peptides) exist as solids at room temperature, there is a probability that they will decompose during heating, as was reported for thymidine (Ptasinska et al. 2006). To overcome this challenge, a novel source and experimental technique were constructed very recently to produce molecular beams of biomolecules (Maddern et al. 2016). As tested for uracil and its derivatives, the source allows the determination of the stability and purity of molecular beams as a function of temperature; these are important factors for obtaining reliable cross sections from crossed-beam scattering measurements. In a typical DEA measurement, the molecular beam collides with the electrons of a specific kinetic energy produced by an electron source. Various types of electron devices (e.g., trochoidal or hemispherical electron monochromators) are used for high resolution DEA studies, and a hot filament or a commercial electron gun are used for lower resolution studies. The anions resulting from the collision are mass selected by a mass spectrometer (e.g., quadrupole, time-of-flight or sector filed mass spectrometers). A typical experimental setup to study isolated molecules in the gas phase, based at the University of Iceland, is shown in Figure 1.

Similar experimental arrangements are also used for studies of biomolecular clusters and for studies of biomolecules deposited onto surfaces (see Section 4). In order to analyse anions, spectra are usually recorded by scanning the incident electron energy, whilst potential voltages applied to the mass spectrometer are fixed for a given ion mass. The ion yields are then plotted as a function of the incident electron energy. In order to calibrate the electron energy scale several calibration compounds with well-known resonant energies for electron attachment processes (e.g., SF_6^- from SF_6, Cl^- from CCl_4, and O^- from CO_2) are used. The experimentally determined position of these resonances allows for the determination of specific points of the energy scale. In addition, to estimate the cross-section values for the anions produced by DEA, the anionic current of a studied biomolecule and the anionic current of the calibration gas with a well-known DEA cross section are measured under the same conditions, i.e., electron current and partial pressure of introduced compounds into the vacuum chamber. However, due to the low precision of pressure measurements of the effusive molecular

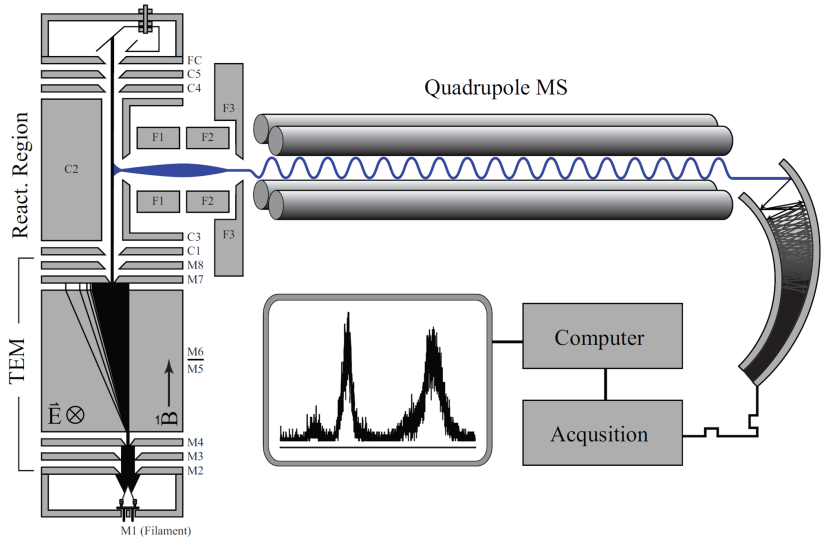

Figure 1. Scheme of the crossed electron-molecule apparatus used for standard DEA studies. It is equipped with a trochoidal electron monochromator (TEM) that consists of a series of electrostatic lenses and slits (M2-M8) under high vacuum conditions, with a pair of magnetic coils outside the chamber. Electrons emitted from a filament (M1) are guided by the electric and magnetic fields to the reaction region (C1-C5), in which the monochromatic electron beam is crossed with the effusive molecular beam introduced to the chamber through an external inlet gas sample system. In this setup, a quadrupole mass spectrometer coupled to a channeltron is used to analyse and detect anionic fragments. The data acquisition system is used to monitor, analyse, and control system units and processes. Reproduced from Ómarsson (2014) with permission from the author.

beam, particularly in the case of powder samples, absolute DEA cross sections for most biomolecules still remain challenging. In addition, as was reported recently (Kopyra & Abdoul-Carime 2015), both absolute and relative DEA cross sections can depend on the temperature of the sample (see Section 3.4). A simple and robust method was designed and used that employed a direct exposure (DE) probe to study gas-phase DEA to larger peptides possessing low volatility (Vasil'ev et al. 2009). The DE probe was constructed from a filament wire and an electrical pin connector fitted into an ion source of a mass spectrometer and then heated by radiation from the hot walls of the ion source kept at ∼500 K; alternatively, the probe holder was heated directly to increase the sample vapour density. Such a design allowed experimentalists to overcome the limited sample volatility with only a slight degree of thermal decomposition.

3. Isolated targets: results

We present here a summary of current data available for elastic, electron and vibrational excitation cross sections, as well as DEA. Results for TCS are mentioned in Section 3.1, because at low energies it is sometimes customary to compare experimental TCS with calculated elastic integral cross sections as the inelastic contribution to the TCS can be,

in this energy range, significantly smaller. As the energy increases, electronic excitation becomes more important and, above 20-30 eV, the ionization cross section becomes significant too. At these energies, it is not longer a good approach to equate elastic and total cross sections. Neither theoretical nor experimental cross section for electron-induced rotational excitation of biomolecules have been reported in the literature. One of the experimental limitations of performing this type of investigation is that the energy spacing of the lowest rotational states is much lower than meV ($\sim 10^{-5}$ eV for the rotational energy levels for isolated nucleobases, see Franz & Gianturco 2014), which is difficult to resolve by current experimental techniques.

3.1. Elastic cross sections

Elastic integral (ECS) and differential (DCS) cross sections are among the most widely studied. From the computational point of view, results can be obtained (for low and intermediate energies) describing only the ground electronic state of the target molecule, thus significantly reducing the complexity and computational demands. All theoretical methods described in Section 2.1 have been employed to determine ECS and DCS. From the experimental point of view, the techniques used are simpler to implement than those requiring the quantification of the energy transferred to the target and/or the identification of its final state.

The main difficulty in evaluating elastic cross sections for most biologically relevant molecules arises from their permanent dipole moment. This is well known to lead to extremely forward-peaked DCS and a divergent cross section within the FNA (Lane 1980). This means both experiment (because of the limited angular resolution and the inability to distinguish between a fully elastic and rotationally inelastic process) and theory are unable to provide an accurate value for the small angle DCS and low energy ECS (Fabrikant 2016) [+]. Comparison between results is hampered by this problem: ECS are determined by extrapolating the experimental DCS or, in the case of calculated ones, by using approximations to complement the partial wave expansion and circumvent the divergence or by excluding very small angles. To avoid this, many authors compare 'uncorrected' theoretical ECS with experimental ones: this normally provides a reasonable agreement, because uncorrected ECS underestimate the contribution of small angles to the ECS and extrapolated experimental ECS tend to do likewise. However, this is not physically correct. Therefore, DCS provide a more

[+] Low energy theoretical methods normally make use of the dipole Born approximation to complement the *ab initio* partial wave expansion (Tennyson 2010, Fabrikant 2016). It is now understood, for example, that the current method used in R-matrix calculations to 'correct' in this way the cross sections overestimates the very small angle contribution to the DCS and therefore the ECS (see Regeta, Allan, Winstead, McKoy, Mašín & Gorfinkiel 2016). The SMC DCS and ECS of Winstead and McKoy are normally not corrected, the DCS SMCPP results from the Brazilian groups are but the ECS tend to be obtained integrating between 1° and 180°. The single-centre expansion results, if corrected, use the same technique as the R-matrix calculations. All 'corrections' imply a (normally implicit) summation over final rotational states.

accurate comparison if small angles (not always measured in experiments in any case) are ignored. One should be aware that, physically, the very large impact parameters implied by very small angles would lead to the electron interacting with more than one molecule, thus putting in question the relevance of a gas-phase cross section for those angles. It should be noted that the focus of many of the theoretical papers presenting calculated ECS is the resonances formed in the collision, not the cross sections themselves. The results below, unless otherwise stated, correspond to 'uncorrected' calculated cross sections.

One of the first, and most investigated biological targets is uracil. Gianturco et al. (2008) (see also Gianturco et al. 2009) presented the contributions of the A′ and A″ irreducible representations to the rotationally summed ECS calculated at SEP level with the single-centre method. Dora et al. (2009) present a comparison of their (corrected and uncorrected) CC R-matrix cross sections with these results and SMC ones of Winstead & McKoy (2006*c*). As expected, when no attempt is made to ensure convergence of their partial wave expansion, the R-matrix cross section agrees reasonable with the SMC one, although the difference in magnitude is significant below 1 eV. When the partial wave expansion is augmented using a Born-type approximation, the agreement is better with the results of Gianturco et al. (2008). The R-matrix DCS for 90° agrees very well with the relative experimental results of Abouaf & Dunet (2005) between 0.5 and 1.5 eV; for lower energies the experimental cross section decreases unphysically. More recently Mašín & Gorfinkiel (2014) obtained very similar (corrected and uncorrected) ECS results to Dora et al. (2009) using the same method and a very similar model and Kossoski et al. (2014) used the SMCPP approach to determine both corrected and uncorrected ECS. These latter ECS are bigger than the R-matrix ones.

Less information is available for the other nucleobases: for thymine and cytosine, cross sections have been calculated at SE and SEP levels using the SMC method (Winstead et al. 2007) and at SE, SEP and CC level with the R-matrix method (Dora et al. 2012*b*). For the reasons explained above, for both molecules the SMC results seem to agree better with the uncorrected R-matrix results. No experiments are available for low energies but, in the range ∼60-500 eV, relative DCS were measured for cytosine and thymine using the crossed-beam method and compared with the theoretical results provided by IAM-SCAR calculations (Colyer et al. 2011); agreement is only fair at the lower end of the energy range but very good elsewhere. Calculations have also been performed for the purinic DNA bases, adenine and guanine (Winstead & McKoy 2006*b*, Dora et al. 2012*a*, Kossoski et al. 2015): at SE, CC and SE/SEP levels respectively. Differences in the A′ and A″ contributions are clearly observable and are probably attributable to the different levels of approximation used. No experiments are available for these targets either.

In terms of the halogenated DNA bases (these targets are interesting because of their radiosesitizing potential, see 5.1.2), Kossoski et al. (2014) present the A′ and A″ contributions to the ECS for 5-fluorouracil, and 5-chlorouracil. The cross sections for both systems (both corrected and uncorrected) are similar in shape and not too different

in magnitude. Kossoski et al. (2015) determined the A′ and A″ contributions to the ECS for adenine and 2-chloroadenine at SE and SEP level: again, both are similar in shape (except at very low energies) with the chlorinated target having a somewhat bigger ECS in the whole energy range. Overall, a good amount of theoretical data, particularly for ECS, is available for the nucleobases. Agreement between different methods is fair, but few experiments are available for comparison.

A related target worth mentioning is pyrimidine: given the higher symmetry of the molecule, accurate calculations are easier to perform, so pyrimidine has been studied as a model for some nucleobases in detail. ECS and DCS have been measured using an EELS setup and calculated with the R-matrix and SMC methods (Regeta, Allan, Winstead, McKoy, Mašín & Gorfinkiel 2016). Figure 2 shows the comparison between theoretical an experimental DCS: there is very good agreement above 20-30°, except for the lowest energy shown (1 eV). The discrepancy at lower energies is due to the long range effect of the dipole moment (not included in SCM calculation and included, but not very accurately, in the R-matrix results) (for more detail see, Regeta, Allan, Winstead, McKoy, Mašín & Gorfinkiel 2016). Theoretical results (corrected and uncorrected) for a wider energy range are presented by Ferraz et al. (2013) and experimental ones by Palihawadana et al. (2011) for energies above 5 eV (and angles 10° to 129°; both of these agree well with Regeta, Allan, Winstead, McKoy, Mašín & Gorfinkiel (2016)).

There is very little work on deoxyribose and ribose. Winstead & McKoy (2006*a*) performed SE calculations on deoxyribose and its monophosphate derivative. The cross sections are similar in shape with the deoxyribose one being smaller in the whole energy range (up to 50 eV). The ECS is also similar to that of THF (that is however, smaller than the deoxyribose one). Calculations have also been performed on ribose and 2-deoxyribose (Winstead & McKoy 2006*a*, Baccarelli et al. 2007, Baccarelli et al. 2009); β-D-ribose and β-D-deoxyribose in the latter publication.

Conversely, the number of studies of elastic scattering from THF is vast. TCS for THF were first measured by Zecca et al. (2005) and ECS calculated by Bouchiha et al. (2006) who performed CC R-matrix calculations (the ECS, since it is Born-corrected, includes some rotational excitation). Agreement is reasonable with the uncorrected ECS, although theory overestimates the cross section at lower energies (note that is now established that Zecca et al. (2005)'s cross section is too low because electrons scattered under small angles were not properly discriminated). The TCS of Możejko et al. (2006), determined using a linear transmission technique, is higher than that of Zecca et al. (2005), although similar in shape. Above 3 eV, this TCS lies between the corrected an uncorrected results of Bouchiha et al. (2006).

Trevisan et al. (2006) and Winstead & McKoy (2006*a*) performed SEP calculations for THF up to 20 eV for ECS and DCS using the Kohn variational and SMC methods respectively (the former results include a correction for the higher partial waves). These cross sections were measured by Colyer et al. (2007) and Gauf et al. (2012) (who also present improved SMC cross sections). DCS were also measured for energies above 6 eV by Dampc et al. (2007). The calculated and measured DCS results in Gauf et al.

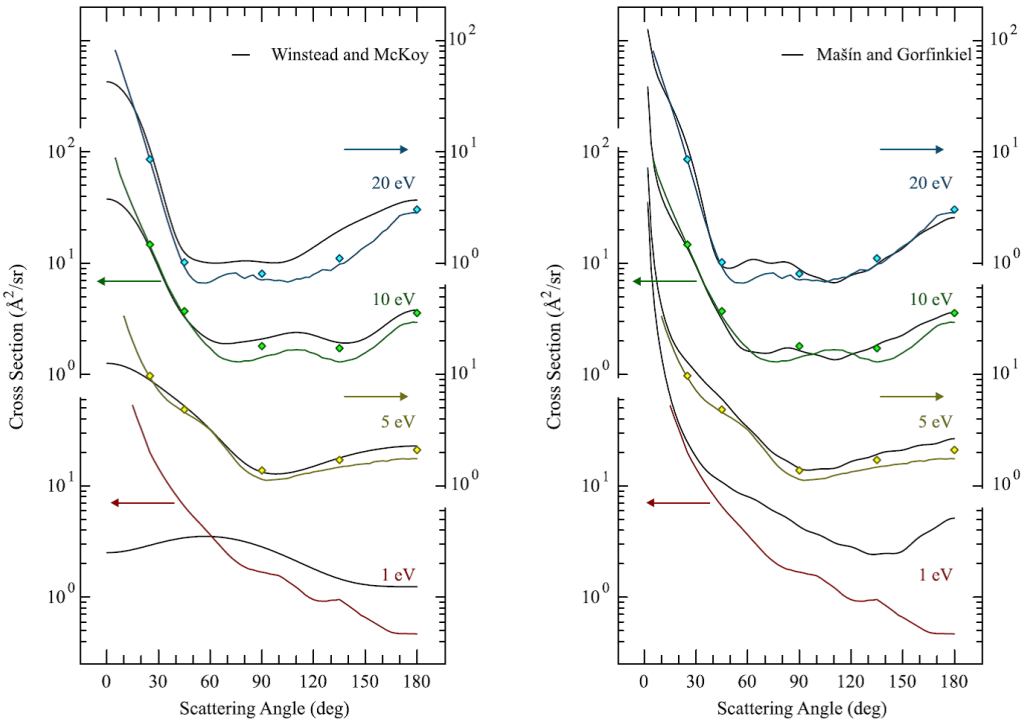

Figure 2. Comparison of the experimental (coloured lines) and calculated (uncorrected) SCM (left panel) and (corrected) R-matrix (right panel) DCS for electgron scattering from pyrimidine. Diamonds indicate sums of elastic and vibrationally inelastic (all modes) cross sections.The experimentally accessible angles are 5° at 10 and 20 eV, 10° at 5 eV, and 15° at 1 eV Reprinted from Regeta, Allan, Mašín & Gorfinkiel (2016) with the permission of AIP Publishing.

(2012) are in good agreement between 30° and 130° (note that the experimental ECS are obtained from DCS extrapolated using a Born-dipole form for small angles and the calculations in the same paper for large ones); agreement is also good with other available data at 2 eV (Allan 2007*b*) and above 6 eV. Their ECS, shown in Figure 3, are also in good agreement up to 30 eV, provided the integration of the SMC theoretical results is carried out between 0.1° and 130°. As expected, the Born corrected R-matrix results overestimate the ECS. More recently, Fuss et al. (2014) determined DCS and ECS in the 10-1000 eV range using the IAM-SCARD method. The DCS (with rotational excitation included) agree very well with experiments above 20 eV; their paper also provide a good summary of THF cross sections for all processes.

The ECS for all deoxynucleosides (deoxythymidine, deoxycytidine, deoxyadenosine, and deoxyguanosine) obtained by Winstead and McKoy using the SCM method are summarised in Winstead & McKoy (2008).

With regards to amino acids, elastic cross sections were determined computationally for scattering from glycine (Tashiro 2008, Panosetti et al. 2010, dos Santos et al. 2012, Nunes et al. 2016), alanine (Panosetti et al. 2010, Fujimoto et al. 2014, Nunes et al. 2016, Fujimoto et al. 2016), proline and valine (Panosetti et al. 2010). The

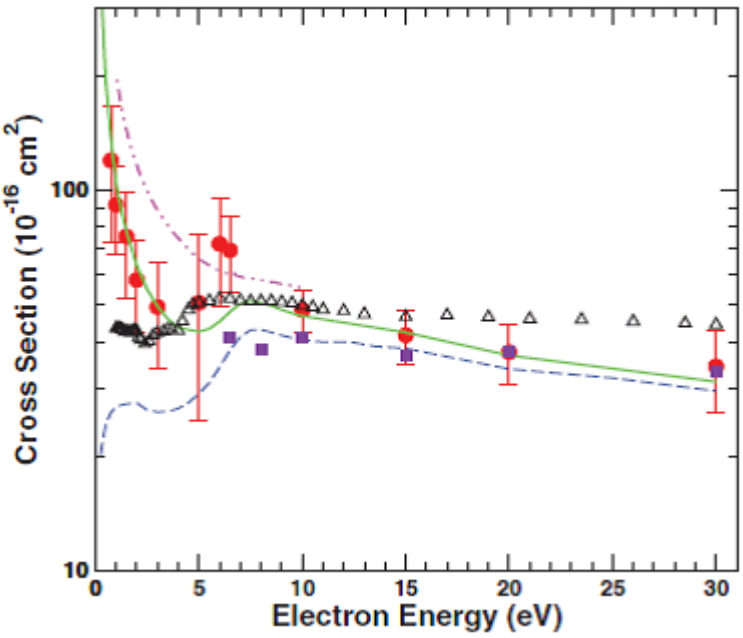

Figure 3. Integral elastic cross sections for electron scattering from THF. Red circles are measurements and the solid green line are calculations from Gauf et al. (2012), both with Born-dipole correction (the dashed blue line is the uncorrected calculation). Other data: violet squares, measurements (Colyer et al. 2007); chained magenta line, calculation (Bouchiha et al. 2006); black open triangles, TCS measurements (Możejko et al. 2006). Reprinted from Gauf et al. (2012) with permission of the American Physical Society.

glycine SEP SMCPP DCS from dos Santos et al. (2012) and the R-matrix ones from Tashiro (2008) agree reasonably for 3 eV in the 60°-140° range and for 6 eV above 50°. The disagreement at small angles may be due to the fact that the calculations include a different number of partial waves (no Born-type correction was added to either calculation). Tashiro (2008) presents a CC TCS that is similar in shape to SEP ECS of dos Santos et al. (2012) although it is smaller in size for the whole energy range shown. Fujimoto et al. (2016) provide corrected R-matrix SEP ECS for nine alanine conformers as well as DCS for several energies. Most of the ECS are smaller in size than that of Panosetti et al. (2010) and the corrected ones of Nunes et al. (2016). This is not inconsistent with the fact that the ECS from Fujimoto et al. (2014) is larger than that of Panosetti et al. (2010) below 4 eV.

To summarise, both integral and differential elastic cross section have been calculated for a number of DNA constituents and their analogues as well as amino acids. Significantly less experimental data is available. The amount of data available varies from significant (for THF) to very limited (for nucleosides) and agreement is, in general, better for DCS than ECS.

3.2. Vibrational excitation cross sections

Only a handful of reports have examined the vibrational excitations of gas-phase biomolecules and provided cross sections. Early experimental data were obtained from EELS for the nucleobases: adenine (Dillon et al. 1989), thymine and 5-bromouracil (Abouaf et al. 2003*a*), cytosine (Abouaf et al. 2004), and more recently for 5 nitro-uracil (Abouaf et al. 2008), and the amino acids glycine (Abouaf 2008, Burean et al. 2008) and alanine (Abouaf 2008). These studies focused primarily on characterising the resonant states observed, i.e., resonance energy and types. For example, energy loss spectra recorded for 5 nitro-uracil at incident energies between 1 and 3 eV showed that essentially the same groups of vibrational modes were excited, but their relative intensities varied (Abouaf et al. 2008). Vibrational excitation at a lower incident energy revealed the excitation of ONO, CNO, NO, and C=O vibrational modes through a π^* resonance, but also of CH and NH stretch modes, indicating that the resonance had some σ^* character. At a higher energy, the last two modes demonstrated that the resonance had a much more pronounced σ^* character (Abouaf et al. 2008).

Similarly, investigations of glycine and alanine at excitation energy of 2 eV, the energy at which transmission experiments in gas-phase demonstrated the presence of resonances (Aflatooni et al. 2001), showed that vibrational excitation primarily concerns the COOH group and CH stretch modes, which indicates that the carboxylic group plays a major role in the formation of the resonance. However, no quantitative studies on cross sections have been performed, largely because of the challenges in precisely estimating the absolute number density of the target. A better estimation of number density can be obtained for samples that are liquids at room temperature. Therefore, research designed to obtain precise cross sections in a wide range of energies for liquid samples that can act as models of biomolecules has increased over the past few years. Electron-impact vibrational excitation for both furan and THF have been experimentally investigated very recently. The energy-loss spectra for furan (Hargreaves et al. 2011, Regeta & Allan 2015), which displayed vibrational excitations, showed that a very broad σ^* resonance indicated for the C-H stretch vibration is generally present at $\sim$ 8 eV in all molecules; thus, this finding can be commonly applied to biomolecules with C-H bonds (Regeta & Allan 2015). In addition, the electron-impact vibrational-excitation of THF has been reported at intermediate incident electron energies between 15 and 50 eV, which significantly extended the cross section data available (Do et al. 2015, Duque et al. 2015).

In the case of pyrimidine, it has been suggested that the target dipole properties do not influence vibrational-excitation, which intrinsically involves the excitation of the nuclear degrees of freedom, in contrast to elastic scattering and electronic-excitation where polarisability and dipole moment play key roles (Jones et al. 2015). Figure 4 shows vibrational integral cross sections (VICS) as a function of the incident electron energy for vibrational excitation in gas-phase pyrimidine.

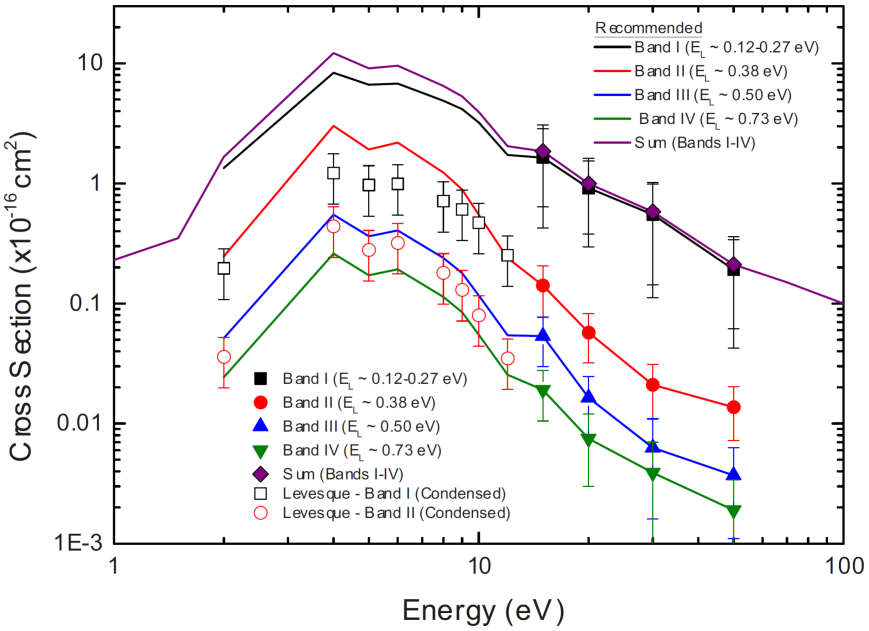

Figure 4. Vibrational integral cross sections as a function of the incident electron energy for vibrational excitation in pyrimidine. The gas-phase unresolved (bands I-IV) VICS from Jones et al. (2015) are represented by closed symbols, and their sum by diamond symbols. The condensed-phase unresolved (band I, band II) results of Levesque et al. (2005) are represented by open symbols. The recommended VICS (solid lines) for each band and their sum are also plotted and were used to simulate charged-particle tracks in liquid pyrimidine (see also Section 5.1.1). Reprinted from Brunger et al. (2016) with permission of Springer.

3.3. Electronic excitation

Fewer results are available for electronic excitation of biologically relevant targets. The reason is twofold: on the theoretical side, the need to model electronically excited states makes the calculations harder and computationally more demanding; not all theoretical methods implemented are able to describe electronic excitation. The experiments are also more difficult, requiring more convoluted 'post-processing' of the data to identify which states are being excited.

Looking at nucleobases, CC calculations using the R-matrix method have been performed for uracil (Dora et al. 2009, Mašín & Gorfinkiel 2014), cytosine and thymine (Dora et al. 2012*b*) and adenine and guanine (Dora et al. 2012*a*). No experiments are available for these targets. However, both experiments and R-matrix calculations have been performed for pyridimine (Mašín et al. 2012, Regeta, Allan, Mašín & Gorfinkiel 2016), with excellent agreement between the cross section (for excitation of a group of states; the experiment can only differentiate 'bands') in the latter work (see Figure 5). The pyrimidine results show that the provision of quantitative data for this process, at least for groups of states and targets that are liquid at room temperature,

is possible.

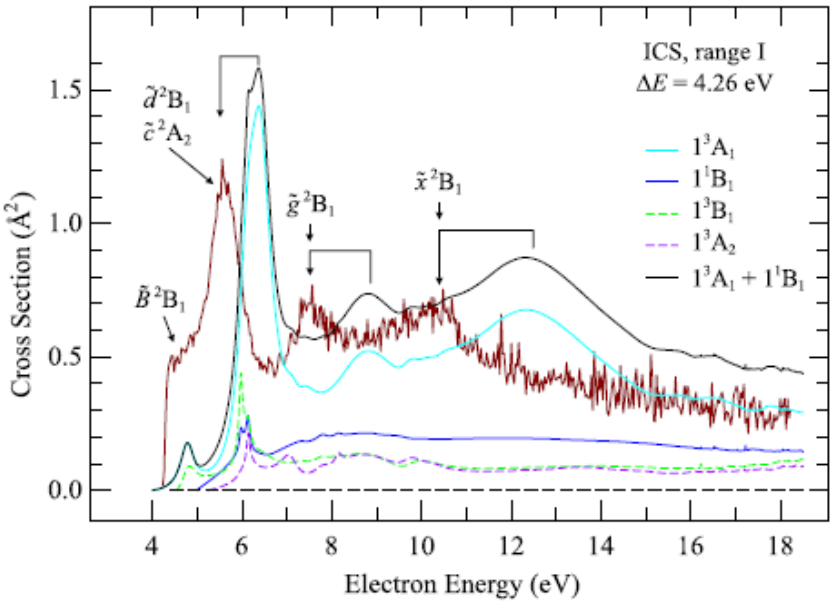

Figure 5. Integral cross section for pyrimidine for electronic excitation of range I (for details, see Regeta, Allan, Mašín & Gorfinkiel 2016). The smooth coloured curves are integral cross sections, calculated with the R-matrix method, for each of the 4 electronic states indicated. The black curve is the sum of the cross sections for exciting the $1\,^3A_1$ and $1\,^1B_1$ states, which contribute to the experimental excitation signal recorded at $\Delta E = 4.26$ eV, shown by the red curve with statistical noise. The $1\,^3B_1$ and $1\,^3A_2$ states are not included in the sum because they lie, respectively, below/above the energy loss of 4.26 eV. The resonances clearly present in both experimental and calculated data are indicated with arrows. Reprinted from Regeta, Allan, Mašín & Gorfinkiel (2016) with the permission of AIP Publishing.

For the sugars/sugar analogues, calculations were performed with the R-matrix method for THF (Bouchiha et al. 2006) for excitation into the lowest 15 states up to 10 eV. Do et al. (2011) measured integral and differential electronic excitation cross sections for energies between 15 and 50 eV. The sum of the experimental partial cross sections at 15 eV is somewhat smaller than the theoretical TICS at 10 eV, pointing at an inconsistency between theory and experiment. More data is available at higher energies.

Tashiro (2008) presented integral cross sections for excitation into the lowest four excited states of glycine as well as angular differential cross sections for these same states at 10 eV. No experiments or calculations for other amino acids are available.

3.4. Dissociative electron attachment and resonance parameters

Dissociative electron attachment (DEA) is experimentally one of the most widely studied processes in electron-biomolecule scattering due to its centrality to radiation damage. Mass spectroscopy enables the identification and quantification of anions produced by

the process. Accurate computational studies are severely limited by the large number of degrees of freedom (electronic and nuclear) that need to be treated. Therefore, most theoretical work has concentrated on investigating the initial DEA step of resonance formation (see Section 3.4.1) and identifying potential products and the mechanism by which they are produced. Some work has also been done on modelling the break-up by reducing the problem to a single degree of freedom (Section 3.4.2). We start by summarising the experimental work on DEA and then briefly describe related calculations.

DNA building blocks: a large number of DEA studies have been performed on gas-phase DNA building blocks and their derivatives over the last two decades (Sanche 2005, Baccarelli et al. 2011). In the case of nucleobases, earlier studies have shown that resonances are present either at subexcitation (< 3 eV) energies or in the energy range between 5-12 eV (Sanche 2005). The higher-energy resonances lead to transient anion fragmentation via opening of the ring structure, while the low energy resonances lead primarily to one or two neutral hydrogen losses, which are accompanied by the perseverance of the ring structure. These DEA studies of nucleobases and their related compounds show a remarkable feature that can be recognised as a common phenomenon, site selectivity (Abdoul-Carime et al. 2004*a*, Ptasinska, Denifl, Grill, Illenberger & Scheier 2005, Ptasinska, Denifl, Scheier, Illenberger & Märk 2005). By tuning the energy of the incoming electron, a specific chemical bond in a molecule can be targeted leading to a specific fragmentation. More recently, this phenomenon has been observed for other nucleobases (Denifl et al. 2007) and their derivatives (Dawley et al. 2015) as shown in Figure 6. These results have significant consequences for the molecular mechanism of DNA strand breaks induced by LEEs. Within DNA, certain H atoms in the nucleobases are replaced by a bond with the sugar moiety thus forming, for example, the nucleoside thymidine; if still present, they may form hydrogen bonds with other nucleobases in Watson-Crick base pairs. Thus, some pathways leading to H loss observed in the gas-phase studies can be suppressed in more complex systems as shown in thymidine (Ptasinska et al. 2006). Nonetheless, comparing the shapes of the signals from nucleobases and more complex systems is essential to identifying the fragmentation patterns. For example, the presence of resonance structure in the ion yields for thymine and thymidine at the same energy and having the same shape indicates that H abstraction in thymidine predominantly occurs at the thymine moiety and, more precisely, at the N3 position, rather than from the sugar moiety (Ptasinska et al. 2006).

In addition to the observation of site selectivity in the DEA process leading to single-bond cleavage within a nucleobase, site selectivity also occurs in multiple bond cleavage. This was demonstrated for the formation of NCO^- from thymine and its derivatives (Silva et al. 2013). This anionic fragment is formed in a sequential decay reaction, in which the dehydrogenated anionic nucleobase is an intermediate product. In this case, the remarkable resonances observed for dehydrogenation and H^- production channels in nucleobases, were preserved for the subsequent decay reaction leading to the

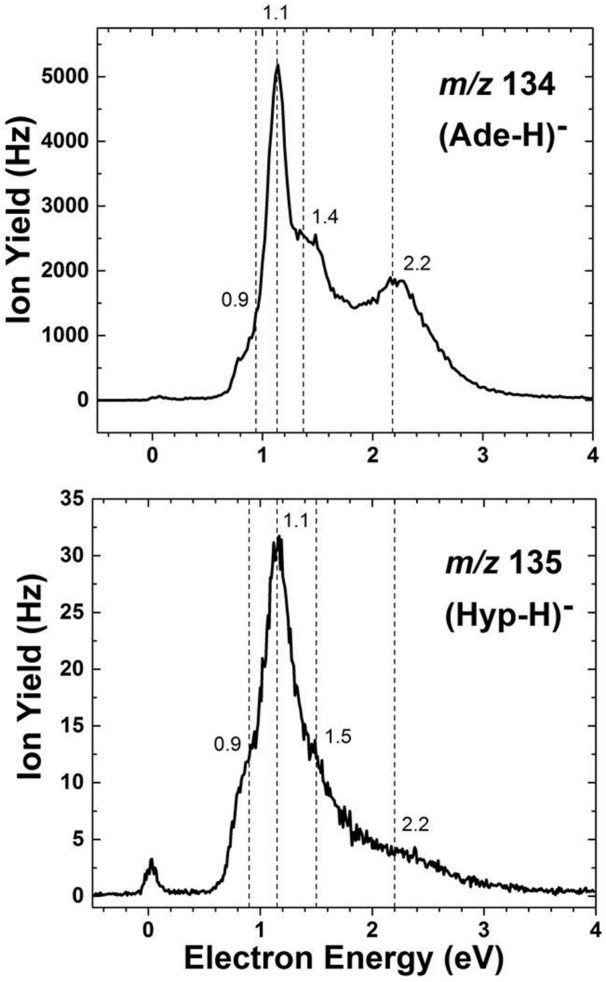

Figure 6. Ion yields as a function of incident electron energy for dehydrogenated adenine ($C_5H_5N_5$, top panel) and its derivative in which the amine group is substituted by oxygen, hypoxanthine ($C_5H_3N_4O$, bottom). Both ion yields exhibit sharp peaks at 1.1 eV and other weaker features below 3 eV marked with dashed lines; however, the relative abundances of these features differ between the two molecules. The possible mechanisms for formation of these anions are discussed in Dawley et al. (2015) Both spectra were taken at an elevated temperature of $\sim$ 450 K thus the peak near 0 eV may arise from the DEA reaction to vibrationally excited molecules ("hot band transition"). Reprinted from Dawley et al. (2015) with the permission of AIP Publishing.

formation of NCO^- as the final product (Figure 7).

In general, the total cross sections for DEA to nucleobases exhibit comparable magnitudes in the energy range for TNI formation (Aflatooni et al. 2006). Importantly, the cross section for the dehydrogenated thymine anion produced via DEA between 393 K and 443 K increased by one order of magnitude, indicating that DEA cross sections are temperature dependent (Kopyra & Abdoul-Carime 2015). Moreover, the extrapolation of these experimental data to a temperature of 313 K shows that the relative DEA cross section for the production of the dehydrogenated thymine anion at

an incident energy of $\sim$ 1 eV decreases by two orders of magnitude and the maximum value reached is $\sim$ 6x10^{-19} cm^2. These cross sections are up to ten times smaller than those for formation of SSBs, whilst the cross section for sugar and phosphate group analogues were even smaller in magnitude.

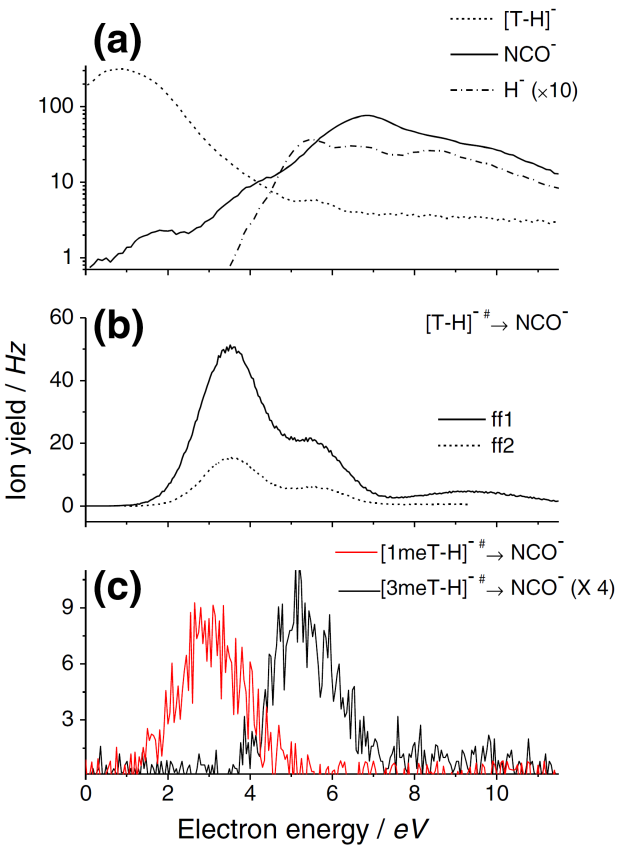

Figure 7. (a) Ion yields for dehydrogenated thymine (dotted line), NCO^- (solid line), and H^- (dashed-dotted line) formed from DEA to thymine upon fast dissociation. (b) Metastable ion yields for the decomposition of the dehydrogenated thymine into NCO^- in the first (solid) and second (dotted line) field free region of the double-sector field mass spectrometer. (c) The same decay reactions as in (b) but for 1-methylthymine (red) and 3-methylthymine (black). Reprinted from Silva et al. (2013) with permission of Springer.

The high fragility of the DNA backbone with respect to the impact of LEEs was observed for 2-deoxy-D-ribose and its RNA counterpart (i.e., ribose) and their analogues (Baccarelli et al. 2011). Dissociation of any P-O-C bond of the sugar-phosphate backbone or of C-C bonds within the sugar can be involved in DNA strand break. DEA at 0 eV is a common property of all monosaccharides (Ptasinska et al. 2004, Baccarelli et al. 2011) but the mechanism is not fully understood. It was proposed to be initiated by the formation of a shape resonance, with the electron attaching to a σ^* orbital of the O-H bond. The DEA mechanisms leading to loss of neutral water are more complex than those in the nucleobases, because they involve the dissociation of multiple bonds

and/or atom rearrangement with simultaneous formation of new bonds. In addition, ribose analogues such as THF and 3-hydroxytetrahydrofuran showed that the DEA cross sections were greatly enhanced by the presence of OH groups (Aflatooni et al. 2006).

The dissociation in sugars involves fragmentation of several different bonds. A proposed mechanism was provided by *ab initio* calculations of the dipole- and valence-bound anionic states of some sugars (Fujita et al. 2016). Since nucleosides can be easily decomposed due to the elevated temperatures necessary for evaporating samples, no experimental data for other gas-phase nucleosides or nucleotides are reported, besides that for thymidine (Ptasinska et al. 2006), cytidine (Kopyra 2012*b*), and 2-deoxycytidine 5-monophosphate (Kopyra 2012*b*). Similarly, due to experimental difficulties, the phosphate group in the gas phase has not been investigated but several compounds involving phosphoric acid derivatives, e.g., dibutylphosphate and triethylphosphate (König et al. 2006), have been examined. The DEA to these compounds leads to P-O and C-O bond cleavage, which correspond to a direct SSB. As is the case for sugars, many fragmentation channels occur close to 0 eV; however, these low-energy channels are most likely driven by the large electron affinity of PO_3 (4.95 eV). The cross sections for DEA to the sugar and phosphate group analogues were relatively small, i.e., about one magnitude lower than those for nucleobases (Aflatooni et al. 2006). However, they reveal that LEE attachment can induce SSBs by electron localisation either on the sugar moiety followed by the electron transfer to the backbone or directly on the phosphate group.

Amino acids: Gas-phase DEA studies designed to investigate amino acids were initiated in parallel with studies of nucleobases, as data on their fragmentation is necessary to obtain a comprehensive picture of the role of LEEs in more complex systems, such as proteins and even DNA-protein complexes. A variety of amino acids has been investigated, including alanine (Ptasińska, Denifl, Candori, Matejčík, Scheier & Märk 2005, Vasil'ev et al. 2006, Abouaf 2008), aspartic acid (Muftakhov & Shchukin 2016), cysteine (Abdoul-Carime et al. 2004*b*), glycine (Gohlke et al. 2002, Mauracher et al. 2007, Ptasinska et al. 2003, Vasil'ev et al. 2006, Abouaf 2008), leucine (Abdoul-Carime et al. 2009), methionine (Kopyra, Szamrej, Abdoul-Carime, Farizon & Farizon 2012), phenylalanine (Vasil'ev et al. 2006), proline (Abdoul-Carime & Illenberger 2004, Sulzer et al. 2008, Muftakhov & Shchukin 2011*b*), serine (Kočišek et al. 2010), tryptophane (Abdoul-Carime et al. 2005, Vasil'ev et al. 2006), tyrosine (Vasil'ev et al. 2006), and valine (Muftakhov & Shchukin 2011*b*, Denifl et al. 2010). The number of high-resolution DEA studies continues to grow.

Similar to nucleobases, ion yields as a function of electron energy exhibit resonances at energies below 15 eV for all amino acids investigated. Studies have found that no parent anion is formed within the detection time of a mass spectrometer, and that the most abundant anionic fragment is formed through H loss from a carboxyl group at energies of 1.5 eV. The same observation has been made for N-substituted amino acids, e.g., N-methylated glycine, N-methylated alanine (Kopyra 2012*a*), and N-acetylglycine (Kopyra, König-Lehmann & Illenberger 2012). However, DEA to

methylated compounds causes relatively strong N-C bond breakage at sub-excitation energies, while the N-Cα (bond between N and C to which a side-chain is attached) breakage for non-methylated analogues diminishes and is accompanied by hydrogen transfer resulting in NH_3 loss (Kopyra 2012*a*). In the case of N-acetylglycine, the DEA peaks shifted to lower energies in comparison to the corresponding anionic fragments from its isolated constituents (glycine and acetic acid) but had much lower intensities. This reduction in the anionic signal was attributed to the larger size of the target compound, and consequently the lower-lying orbitals involved in the DEA process and the higher number of vibrational degrees of freedom (Kopyra, König-Lehmann & Illenberger 2012).

Moreover, these gas-phase studies of modified amino acids were expanded to include electron attachment ethyl (Et), isopropyl (i-Pr), and t-butyl (t-Bu) esters of glycine, alanine, and phenylalanine (Vasilev et al. 2007). The most abundant and characteristic fragments produced by DEA to esters were associated with the C-termini, i.e., [M-X], COOX, and OX (X is methyl, Et, i-Pr, or t-Bu). The generation of the anion due to X loss was found to be very efficient in the low-energy range and achieved maximum intensity for loss of i-Pr and t-Bu esters. In contrast, two other anionic fragments were formed at higher energies with relative intensities similar to those for all three amino acids (Vasilev et al. 2007).

Despite the fact that a number of experimental investigations of DEA to several amino acids have revealed that hydrogen loss occurred from the carboxyl group, the exact reaction pathway has long been under debate. A possible mechanism involves electron attachment to a π^* orbital of the C=O bond of the carboxyl group, and subsequent electronic coupling with the antibonding σ^* orbital that leads to dissociation of the O-H bond (Ptasinska et al. 2003). An alternative mechanism involves the decay of vibrational Feshbach resonances formed via dipole-bound anion states (Vasilev et al. 2007, Abouaf 2008). Based on a comparison with resonance of their analogues $[M\text{-}X]^-$ for amino acid esters, it was proposed that the dehydrogenated anions are produced at the lower adiabatic state via hydrogen-atom tunnelling through the barrier that separates a dipole-supported minimum and repulsive valence state. In contrast, the $[M\text{-}X]^-$ anions are produced from the upper adiabatic state in which the energy of the valence σ^*(OX) resonance exceeds the bond dissociation energy of the neutral molecule without penetration of the barrier (Vasilev et al. 2007). More recently, a mechanism in which the electron is attached directly to the short-lived, repulsive σ^* orbital of the O-H bond, which exhibits a very broad resonance with a width of approximately 6 eV (Gallup et al. 2009, Vizcaino et al. 2012) seems to have been confirmed (see Section 3.4.1). The ion yield for the dehydrogenated molecular anion reveals only the lower energy tail of this resonance (up to ∼2 eV) because of effective electron autodetachment, which also involves vibrational excitation of the remaining neutral molecule at higher energies (Gallup et al. 2009, Vizcaino et al. 2012).

There is also a possibility that higher energy resonances are formed at ∼5-6 eV, which involve hydrogen loss from other sites, e.g., the amide, rather than

the carboxyl group, for all amino acids studied. Interestingly, metastable decay of dehydrogenated amino acids was found in the region of 4.58 eV for valine (Muftakhov & Shchukin 2011*b*, Flosadóttir et al. 2007) and proline (Muftakhov & Shchukin 2011*b*), and different fragmentation pathways and the structure of products were considered. Another peculiar observation in the resonance formation of dehydrogenated amino acids is that the ion yield alters significantly depending on the position of the amino group in the molecule, as was shown by comparing DEA processes to α- and β-isomers alanine (Vizcaino et al. 2011).

In the case of methionine, which in contrast to others, is a sulphur-containing amino acid, DEA also leads predominantly to H loss but shows cleavage of the C-S bond, which results in many sulphur-neutral fragments. One of these fragments is highly toxic methanethiol that is produced at an energy that approaches 0 eV (Kopyra, Szamrej, Abdoul-Carime, Farizon & Farizon 2012). In addition to these high-resolution DEA studies, which used electron monochromators (Section 2.2), high-resolution mass analyses have been performed for a few aliphatic amino acids: alanine (Shchukin et al. 2010), glycine (Shchukin et al. 2010, Mauracher et al. 2007), proline (Sulzer et al. 2008), and valine (Shchukin et al. 2010). These studies led to more precise identifications of anionic fragments that have the same nominal masses as those probed previously, both experimentally, by targeting deuterated and/or methylated analogues, and by predicting their structures from the enthalpies of formation of possible products. Accurate mass measurements of anionic fragments showed that N- and C-terminal anions resulting from DEA to amino acids that have the same masses exhibit resonances at different electron energies (Shchukin et al. 2010).

Peptides: To further investigate LEE interactions relevant to life, the range of biomolecular targets was recently expanded to larger systems containing amino acids such as peptides and proteins. These DEA studies were performed for short peptides, including dipeptides: glycyl-glycine (Muftakhov & Shchukin 2011*a*), alanyl-alanine (Muftakhov & Shchukin 2011*a*, Alizadeh et al. 2011, Gschliesser et al. 2012, Puschnigg et al. 2013), glycyl-alanine (Muftakhov & Shchukin 2011*a*, Shchukin et al. 2012), and alanyl-glycine (Kopyra et al. 2013); tripeptides, e.g., trialanine (Vasil'ev et al. 2009, Puschnigg et al. 2014) and glycine-glycine-leucine (Vasil'ev et al. 2009), and higher order tetra-, penta-, hexa-peptides, containing alanine and methionine (Vasil'ev et al. 2009). In addition to the relatively short homo- and hetero peptides, studies were also performed for peptides that occur naturally, such as methionine enkephalin and substance P (neuropeptide) (Vasil'ev et al. 2009).

Dipeptide studies have shown that LEE attachment produces effective fragmentation over an extended electron energy range below 15 eV, with the same order of magnitude for DEA cross section as amino acids (10^{-19} cm^2 for the dehydrogenated anions, Muftakhov & Shchukin 2011*a*). As for other amino acids, the alanine dipeptide and its cyclic derivative (Alizadeh et al. 2011), alanine anhydride, fragmented into many anions (approximately 30 for both samples), with the abundant formation of dehydrogenated anions below 2 eV. Further, high resolution DEA studies of dialanine revealed

two distinct resonances at 0.81 and 1.17 eV in the ion yield linked to H loss, which occurred by abstraction of a hydrogen atom from the carboxyl and amide groups, respectively (Gschliesser et al. 2012). However, the methylation of the carboxyl group induced a resonance shift to higher electron energy, with the lowest lying resonance observed at 2.4 eV (Puschnigg et al. 2013). This observation is significant with respect to site selectivity of hydrogen loss from isolated gas-phase biomolecules, as was observed clearly for nucleobases (Denifl et al. 2007, Ptasinska, Denifl, Scheier, Illenberger & Märk 2005, Ptasinska, Denifl, Grill, Illenberger & Scheier 2005). In the case of dialanine, the resonances' shapes and positions were altered not only by blocking specific sites, but the energetics were modified strongly (Puschnigg et al. 2013) as shown in Figure 8.

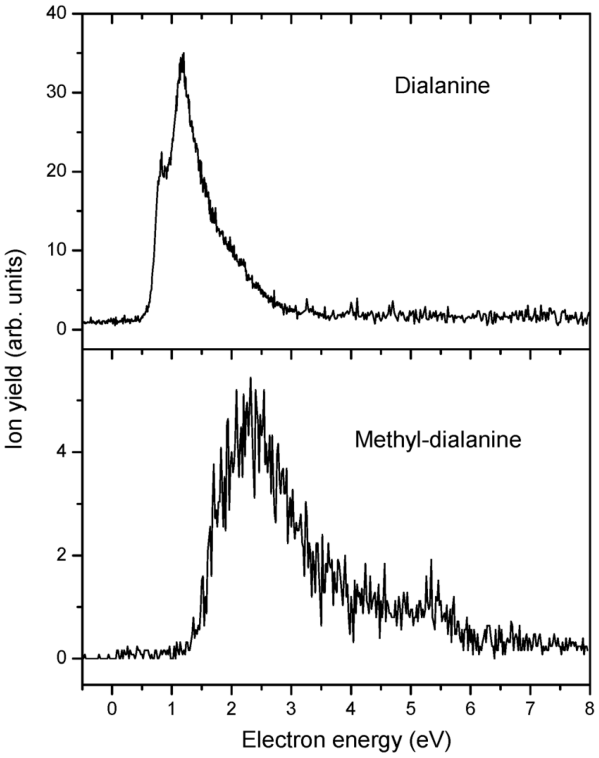

Figure 8. Comparison of the dehydrogenated anion yields for dialanine (upper panel) and dialanine methylated at the carboxyl group (lower panel), which shows the expected disappearance of the 1.17 eV resonance linked to H loss from the carboxyl group in the latter due to this position being blocked by the methyl group. However, the resonance at 0.81 eV linked to H loss from the amide group is not present for methylated dialanine either, despite the site available for H loss. A shift in the threshold for H loss upon methylation is discussed based on quantum chemical calculations in Puschnigg et al. (2013). Reproduced from Puschnigg et al. (2013) with permission from the PCCP Owner Societies.

The resonance positions observed for other fragments from dialanine were in close agreement with previous calculations of the vertical attachment energies required to break the N-Cα and peptide (amide) bonds (Sobczyk et al. 2005). These calculations

of various σ^* and π^* orbitals of dialanine predicted that the N-Cα cleavage involves formation of the central carbonyl C=O π^* anion and electronic coupling to the dissociative σ^*N-Cα bond. This reaction is accessible for electron attachment that occurs with energies near 2.5 eV. In contrast to this indirect mechanism of N-Cα cleavage, the direct mechanism, in which the electron is captured into any of the σ^* orbitals, is accessible only with energies greater than 6 eV (Sobczyk et al. 2005). Other calculations of the dipole moment for dialanine indicated that the dehydrogenated anion may be formed via dipole-bound states, as the dipole moment for its conformers was in the range of 4-5 D. In contrast, for alanine anhydride conformers, the dipole moment has subcritical values of 1 D, insufficient for the formation of dipole-bound anions (Alizadeh et al. 2011).

DEA studies of other dipeptides confirmed rich fragmentation patterns that involve simple bond cleavage and rearrangement processes that are primarily reactions of hydrogen transfer (Muftakhov & Shchukin 2011*a*). This transfer mechanism is possible because strong intra-molecular hydrogen bonds are present initially in some conformers of dipeptides, or are formed during transit negative ion formation. Interestingly, for alanyl-alanine and glycyl-alanine, the metastable decays of two anions produced at higher electron energies (5 eV) via H or COOH loss (Muftakhov & Shchukin 2011*a*, Gschliesser et al. 2012, Shchukin et al. 2012) from dipeptides were observed. This had been reported earlier only for H loss from amino acid monomers (Denifl et al. 2010, Muftakhov & Shchukin 2011*b*) and might be due to accumulation of the internal energy of the larger system, whose decaying ion has a higher number of active vibrational degrees of freedom (Muftakhov & Shchukin 2011*a*). Moreover, a statistical approach was used recently to reveal the decay mechanism of these two metastable ions of dipeptides: Shchukin et al. (2012) found that the metastable decay can proceed through simple bond cleavage, intramolecular rearrangement or two subsequent dissociative reactions that lead to the formation of fragment ions with different spatial structures. These most probable fragmentation channels were characterised by the lowest energies and minimal structural changes of the dissociating anions that avoided complicated rearrangements and isomerisation processes. Further, in contrast to glycyl-alanine (Muftakhov & Shchukin 2011*a*), DEA to alanyl-glycine exhibited new resonant features at an energy threshold of 0 eV (Kopyra et al. 2013).

Experimental studies of trialanine that used a high-energy resolution monochromator indicated that formation of anionic fragments is most abundant up to electron energies of ≈4 eV (Puschnigg et al. 2014). Similar to the isolated monomer (Ptasińska, Denifl, Candori, Matejčík, Scheier & Märk 2005, Vasil'ev et al. 2006, Abouaf 2008) and dimer (Muftakhov & Shchukin 2011*a*, Alizadeh et al. 2011, Gschliesser et al. 2012, Puschnigg et al. 2013) of alanine, there is no evidence that a bound molecular anion exists on mass spectrometric detection timescales, and the dehydrogenated anion is one of the fragment anions observed. The thermochemical calculations performed on the threshold energies for formation of anionic products for trialanine showed a strong dependence on the tripeptide conformers, including internal hydrogen bonding of the

carboxyl hydrogen with the oxygen of the adjacent amide group. In contrast to the dialanine and alanine, the cleavage of the N-Cα bond in the tripeptide appears at an electron energy near 0 eV (Puschnigg et al. 2014). This peptide breakage was proposed to be energetically possible only via a complex reaction, including a subsequent proton transfer, as was also suggested for dipeptides (Muftakhov & Shchukin 2011*a*).

As mentioned in Section 2.2, gas-phase DEA investigations are limited with respect to the size of the molecules studied, primarily because larger biocompounds require higher temperatures for evaporation in the oven, and unfortunately, these can decompose a sample. Fragmentation of several neutral model peptides and two naturally-occurring peptides was studied with the DE probe at two fixed electron energies, i.e., 1-2 and 5-6 eV, which correspond to energy ranges at which DEA was observed for most fragments for amino acid monomers and dipeptides. Highly resolved mass spectra indicated the occurrence of two typical anions at the lower energy range for alanine polypeptides (up to hexapeptide), i.e., the dehydrogenated anion due to H loss and the anions associated with breakage of the N-Cα bond accompanied by hydrogen atom loss (Vasil'ev et al. 2009). The relative ion yields of these two anions depend on the peptide size: the abundance of the dehydrogenated anion decreased, whilst that for the other anions increased with increasing peptide size. In contrast, mass spectra recorded at the 1-2 eV range showed a total quenching of the ion signal for the dehydrogenated channels in the case of the two naturally-occurring peptides, methionine enkephalin and substance P. Different mechanisms for N-Cα bond cleavage were associated with larger amide-containing peptides, despite clear evidence of the formation of the anion due to cleavage of this peptide bond. The fragmentation pathways for methionine enkephalin, and substance P resembled those detected for the model peptides via mass spectrometer (Vasil'ev et al. 2009).

It is worth noting that another experimental approach has been applied in conjunction with aerosol mass spectrometry to probe LEE interactions with short peptides, in which photoelectrons with energies of $\sim$0-1 eV were attached to cysteine, two dipeptides that contain the cysteine residue (cysteinyl-glycine and glutamyl-cysteine), and the biologically relevant tripeptide, glutathione (Geddes et al. 2009). However, the results from this experimental approach indicated the absence of the anions formed due to N-C(α) bond cleavage, which could be attributed to the different environments of peptides in aerosol and isolated peptides in vacuum. Finally, smaller compounds containing peptide linkages were also investigated, such as formamide (Hamann et al. 2011) and N-methyl formamide (Dawley & Ptasińska 2014). Interestingly, both molecules, as well as the peptides, e.g., dialanine (Alizadeh et al. 2011, Muftakhov & Shchukin 2011*a*), showed a double peak resonant structure for anions that corresponded to the peptide bond breakage in the region between 5-8 eV. This indicates that the energy required to form a TNI and cleave this bond is very similar for all of these molecules and depends only slightly on the size of the target. Thus, the DEA process for this reaction is highly localised and depends only on the chemical nature of the covalent bond with a minor influence of the molecular environment.

3.4.1. Resonance characterization Computational work has focused on the study of resonances, their energy (position) and lifetime (width) and their link to DEA products. Most work has centred on shape resonances, for which the calculations are simpler and less computationally demanding since they only require the inclusion of the target ground state.

The shape resonances in DNA bases have been widely studied. Some of the more recent work on nucleobases and halogenated nucleobases has been described in Section 3.1, where elastic scattering calculations are discussed. A summary of the energy of the lowest three π^* resonances calculated before 2008 with a number of methods (single-centre, Schwinger and R-matrix eigenchannel) is provided by Winstead & McKoy (2008). The calculated positions tend to be higher than those determined experimentally (Aflatooni et al. 1998) for well known reasons: in general, the polarization effects are not fully described, or (particularly for the third resonance) the character of the resonance is partially core-excited so elastic calculations do not describe it very well.

The R-matrix method has been used to determine parameters for all shape and some core-excited resonances in all DNA bases at equilibrium geometry (Dora et al. 2009, Dora et al. 2012*a*, Dora et al. 2012*b*, Mašín & Gorfinkiel 2014). The positions of the π^* shape resonances calculated at CC level agree better with experiment (Aflatooni et al. 1998) than any previous work for cytosine and thymine whereas for guanine and adenine, the agreement is similar to that of the Schwinger SEP results (Winstead & McKoy 2008). Dora et al. also identify: three Feshbach-type resonance for uracil, a fourth π^* resonance in the pyrimidinic bases with some core-excited character, indications of higher-lying shape resonances (of a different symmetry to the π^*) in thymine and two Feshbach-type resonance for adenine above 5 eV. Mašín & Gorfinkiel (2014) found 10 core-excited shape and two Feshbach resonances for uracil, the latter of a different symetry to those reported by Dora et al. (2009). Given that the same method and the same software suite were used in both calculations, this difference was ascribed to: (i) the fact that Dora et al. (2009) did not attempt to identify all the resonances present in the system (therefore 'missed' many of the core-excited shape resonances); (ii) the correction of a bug in the software used. It is worth highlighting that a recent experimental-theoretical work (Regeta, Allan, Mašín & Gorfinkiel 2016) has confirmed the accuracy of the R-matrix calculations to reproduce core-excited resonances in pyrimidinic systems (see Figure 5).

No significant attempt has been made to link the core-excited resonances to DEA cross sections, except for uracil (Mašín & Gorfinkiel 2014) using only equilibrium geometry calculations.

SMCPP calculations for uracil and halouracil confirmed (Kossoski et al. 2014, Kossoski & Varella 2015) that halo-substitution stabilises (lowers the energy) the π^* (particularly the lowest one that becomes a bound state for some of the systems) and the shape σ^* resonances; results are in qualitative agreement with Scheer et al. (2004). In addition, Kossoski & Varella (2015) discuss possible explanations for the absence of hydrogen elimination signals in DEA to bromo- and iodouracil (this signal is present

in uracil and flouro- and chlorouracil) . Kossoski et al. (2015) calculated resonance positions for the shape resonances of 2-chloroadenine using the SMCPP method, finding again that the π^* resonances are stabilized; they link anion production to shape and vibrational Feshbach resonances.

The effect of halogenation has also been studied (again, using the SMCPP method) for pyrimidine (Barbosa & Bettega 2013) where similar results have been obtained (stabilization of π^* resonances and presence of σ^* resonance localised in the halogen-carbon bond) in agreement with experimental results (Modelli et al. 2011).

Resonance formation has been studied for amino acids, both theoretically and by means of ETS (the latter for glycine, alanine, phenylalanine, tryptophan, and proline by Aflatooni et al. 2001). In the case of glycine, Tashiro (2008) identified a π^* resonance around 3.4 eV and many core-excited resonances above 5 eV. These results are consistent with the energy ranges in which anions are produced in DEA experiments (Gohlke et al. 2002, Ptasinska et al. 2003, Mauracher et al. 2007). Fujimoto et al. (2016) used the R-matrix method at SEP level to study the shape resonances of nine alanine conformers. Two resonances are present: a lower energy one of π^* character around 2.6 and 3.1 eV and a broader, higher one, perhaps of mixed character and associated to a σ^* orbital, with energy in the 9-9.7 eV range. The experimental DEA results of Scheer et al. (2007) seem to show, however, the presence of three peaks at somewhat different energies from those calculated. For cysteine (and its oxidized dimer cystine), single-centre expansion calculations were performed to study the shape resonances as a function of several single-bond stretches (Wang et al. 2011).

Recent work demonstrates the ability of adapted quantum chemistry methods to describe resonances in biomolecules and provide information on their energy and lifetime. For example, the complex absorbing potential (CAP)/symmetry adapted cluster-configuration interaction (SACCI) method reproduce the ETS position of the low π^* resonances for DNA bases (calculations for substituted forms are also presented, Kanazawa et al. 2016). Other groups have applied similar stabilization techniques to halopyrimidines (Cheng et al. 2016) to study shape and core-excited resonances using the polarized continuum method (PCM) to model the effect of water when the molecules are in solution. Also worth mentioning is the CAP-EOM-EA-CCSD technique, so far applied to p-benzoquinone (Kunitsa & Bravaya 2016), a molecule of great biological interest since quinones are involved in electron-transfer chains in biological systems. These works need to be distinguished from those that apply (unmodified) conventional bound state techniques to obtain resonance energies. Although it seems that, through a careful choice of basis set and other parameters, reasonable results are obtained for the energies of some resonance in biomolecules (e.g., uracil), the risk of variational collapse is ever present (Herbert 2015). One should therefore be wary of basing a proper understanding of resonances on the use of these methods alone. A summary of quantum chemistry techniques appropriate for the study of resonances can be found in Herbert (2015).

3.4.2. Inclusion of nuclear motion Determining computationally all the products of DEA for a particular collision requires the treatment of all nuclear degrees of freedom, as well as the characterization of all relevant resonances in the system as a function of all nuclear coordinates. This task has only been achieved (in full dimensionality) for very small molecules (e.g., H_2O). For biologically relevant molecules, only one dimensional approaches have been used. The most sophisticated work on DEA including nuclear motion has been performed by Fabrikant and collaborators using the resonant R-matrix theory (Lane & Thomas 1958, Fabrikant 1991) and the non-local complex potential approach (Domcke 1991). The process investigated has been dehydrogenation (i.e., formation of the molecular anion from which an H atom has detached) of glycine (Gallup et al. 2009), uracil and thymine (Gallup & Fabrikant 2011) and aminobutanoic acid (Vizcaino et al. 2012). In the case of uracil, the detachment of the hydrogen atom attached to both nitrogens has been modelled, including the effect of the dipole-bound state and the vibrational Feshbach resonances.

The empirical study of glycine (Gallup et al. 2009) demonstrated that H loss around 1-1.3 eV proceeds via direct electron attachment to a very short-lived (extremely wide) valence σ^* resonance. This mechanism was confirmed for the closely related formic acid by experiments using deuterated targets (Janečková et al. 2013). H loss to formic acid has been extensively studied computationally and experimentally: two mechanisms were proposed, one involving attachment to a π^* resonance and coupling to an energetically close σ^* resonance (Rescigno et al. 2006) that requires out of plane motion of the H and one that only requires attachment to a very wide σ^* resonance (Gallup et al. 2009). Janečková et al.'s experiments showed little change in the cross section when OH was replaced with OD, hence demonstrating the H loss did not involve out of plane motion. The very wide σ^* resonance involved in this DEA process is extremely difficult to detect in *ab initio* calculations where it is normally hidden by the dipole and polarization enhanced non-resonant contribution to the scattering. (We refer the reader to Bald et al. (2017) for a more detailed discussion of the process and the work done to investigate it).

Other researchers have stopped short of explicitly modelling the nuclear motion in their calculations but have looked at the evolution of resonances as a function of a specific nuclear coordinate, as a way of determining whether they lead to dissociation or not. Examples of this type of work are single-centre calculations for amino acids like the one for cystine and cysteine (Wang et al. 2011) already mentioned and others performed by the Rome group (a sumary description can be found in Panosetti et al. 2010). In addition, single-centre calculations (Gianturco et al. 2008) were performed for uracil and SMCPP ones for 5-chlorouracil Kossoski et al. (2014). In these works, fixed-nuclei calculations for a number of geometries were carried out. The work on chloruracil, for example, shows how the stretching of the C-Cl bond stabilizes the σ^* resonance significantly more than the π^* (as expected) making a coupling between the two, and therefore a C-Cl bond breaking mechanism in which the electron is initially trapped in the π^* resonance possible (this σ^*-π^* coupling mechanism is well known from DEA to

uracil as explained by Scheer et al. 2004).

4. Aggregates

Early on in the study of electron scattering from biologically relevant molecules, it was recognised that gas-phase/isolated molecule studies, in neglecting the influence of the environment in the collision, may not be providing a wholly accurate picture. Biological matter is condensed matter, and all electron interactions with it will be influenced by the environment *. Even in experiments with 'isolated' DNA strands (like the seminal work of Boudaïffa et al. 2000), structural water molecules are involved.

In order to account for the condensed character of the cell, many experiments have been performed for thin films of a specific molecule (deposited on a substrate and even covered with layer(s) of H_2O) but we will not discuss these here. For detailed reviews and a description of more novel techniques (like DNA origami, used to investigate the dependency of the damage on the sequence and composition of a short DNA strand, Keller et al. 2014), we refer the reader to earlier (Sanche 2005, Naaman & Sanche 2007) and a recent (Alizadeh et al. 2015) publication; the counterpart theoretical work has so far focused only on small molecules.

Another way of understanding the effects of the environment is to look at electron scattering from molecular clusters. Clusters can be seen as bridging the complexity gap between gas and condensed phase. The aim of the work on clusters is mainly to understand how hydration (or water solvation) affects the electron induced processes. Earlier work was performed on electron induced dissociation of positively charged clusters: for example, hydrated peptides (Prell et al. 2008), clusters of the amino acid derivative betaine (Feketeová & O'Hair 2009) and tryptophan, etc.. Work was also performed on dimers of non-biological molecules (Gianturco et al. 2005, Allan 2007*a*, Freitas et al. 2011, Gorfinkiel & Caprasecca 2012), pure water clusters (Caprasecca et al. 2009) and mixes (Freitas et al. 2009, Freitas et al. 2013). More recently, work is being carried out for neutral clusters containing a biomolecule and one or several water molecules.

Another important question is how, for example, electron attachment to DNA components is related to attachment to a DNA strand; in particular, how predictions for the latter can be made investigating the former. Caron et al. (2009) and Caron et al. (2008) used a multiple-scattering approach to combine R-matrix eigenchannel scattering data for DNA constituents and investigate this effect in electron attachment to a DNA base-pair decamer (including structural water).

* In a biologial environment, free electrons will eventually be solvated and have little damaging potential. Before the formation of solvated electrons, pre-solvated electrons with a finite lifetime are formed; these pre-solvated electrons can produce DNA damage by dissociative electron transfer (Wang et al. 2009), a reaction essentially similar to DEA that is initiated by the transfer of the pre-solvated electron to the target molecule (Alizadeh & Sanche 2012).

4.1. Theoretical approaches

Ab initio calculations of electron scattering from small clusters containing a biologically relevant molecule are difficult due to the size of the calculation. Some work, however, has been performed using the R-matrix method. SE and SEP calculations investigated shape resonances in thymine·$(H_2O)_n$ (Ryszka et al. 2015, Sieradzka & Gorfinkiel 2017). This work is at the moment limited to processes and resonances that involve the electronic ground state of the cluster only.

Work has also been performed to understand DEA in microhydrated nucleobases. In particular, H loss has been studied for a cluster of uracil/thymine and five water molecules (Smyth et al. 2014). The methodology applied here is based on using a combination of techniques: the non-local complex potential method mentioned in section 3.4.2 and the multiple scattering approach, standard quantum chemistry techniques to determine the vertical attachment energies of the resonance of interest and standard scattering techniques to generate the T-matrices needed for the multiple scattering approach. The results seem to indicate that solvation increases the DEA cross section for dehydrogenation. The approach is currently limited to 1-dimensional DEA.

Finally, we mention that some research has been performed combining molecular dynamics calculations and density functional theory to model electron attachment to DNA nucleotides in an aqueous solution and the energy involved in bond cleavage (e.g. McAllister et al. 2015).

4.2. Experimental approaches

Electron scattering experiments using biomolecular clusters as a target system have been performed using crossed electron-molecular beam setups coupled to a mass spectrometer as described in Section 2.2 for DEA studies. However, such setups have been modified by attaching a source for microhydrated biomolecules. There have been reports about tests of several designs to investigate the effect of solvation on electron scattering of hydrated nucleobases (Fröstel et al. 2015, Kočišek, Pysanenko, Fárník & Fedor 2016) and model molecules (Neustetter et al. 2015) (we briefly summarise the experiments performed in the next Section).

One of the designs for biomolecular aggregates consists of two reservoirs, one for water which, when heated, produces water vapour that expands through the tube into the second reservoir containing a biomolecule powder (Fröstel et al. 2015). The biomolecule reservoir is typically heated more than the water reservoir and the clusters are formed in a conical-shaped nozzle. The water-biomolecule clusters form both because of the co-expansion of mixed species and because of the attachment of molecules to pre-formed clusters after the expansion, so called "pick-up". The effectiveness of this source was tested by detecting positive ions for water-adenine and water-uracil mixtures ionised by 70 eV electrons and recording the resulting ions with a quadrupole mass spectrometer. This experimental setup produced five different types of clusters: protonated water

clusters of up to 16 molecules of intact water, protonated and non-protonated uracil monomers solvated with up to 10 water molecules, and protonated and non-protonated hydrated uracil dimers.

In another design, a mixture of humidied buffer gas (helium or argon, Kočišek, Pysanenko, Fárník & Fedor 2016, Kočišek, Grygoryeva, Lengyel, Fárník & Fedor 2016) and nucleobase vapour expand into the vacuum, where they collide with a tunable-energy electron beam, resulting in negatively charged ions that are detected by a reflectron time-of-flight mass spectrometer. The humidified buffer gas passes through a reservoir filled with a sample powder. Similar to the design described above, the clusters are produced in a conical nozzle, which is kept at a slightly higher temperature to prevent sample condensation. This setup produces only single microhydrated biomolecules as opposed to the other design, which yielded five types of clusters.

We also mention briefly that a few experiments have been performed for amino acid clusters in helium nanodroplets (da Silva et al. 2010, Weinberger et al. 2016).

4.3. Aggregates: results

We highlight two recent experimental works that look at DEA measurements in molecular clusters.

Using the setup outlined above, Kočišek, Pysanenko, Fárník & Fedor (2016) investigated DEA products of clusters of a single thymine or uracil molecule with a few water molecules for electron energies below 3.5 eV. Figure 9 shows results for two different 'amounts' of microhydration obtained performing the experiments under two different sets of conditions. The most noticeable result is the complete disappearance of the dehydrogenated anion for both nucleobases. This result seems to contradict Smyth et al. (2014). However, the authors' hypothesis is that the quenching is due to the presence of water preventing the H atom from detaching (rather than changes to the electron attachment process itself), an effect not included in the calculations of Smyth et al. (2014). More work is clearly needed to elucidate the quenching mechanism.

In the second experiment, DEA to pure and hydrated clusters of pyrimidine was investigated (Neustetter et al. 2015). The yield of dehydrogenated pyrimidine anion is different between the two types of cluster and very different from gas-phase pyrimidine. The yield of the pyrimidine dimer anion is similar for both types of cluster below 2 eV whereas for higher energies is only observed for pure clusters; the latter is also the case for the pyrimidine anion. A caging ('steric shielding') effect due to the water molecules is suggested as a possible explanation of the reduced/quenched yields for the hydrated clusters (or, alternatively, the emission of the captured electron leaving the water-pyrimidine complex in an electronically excited state).

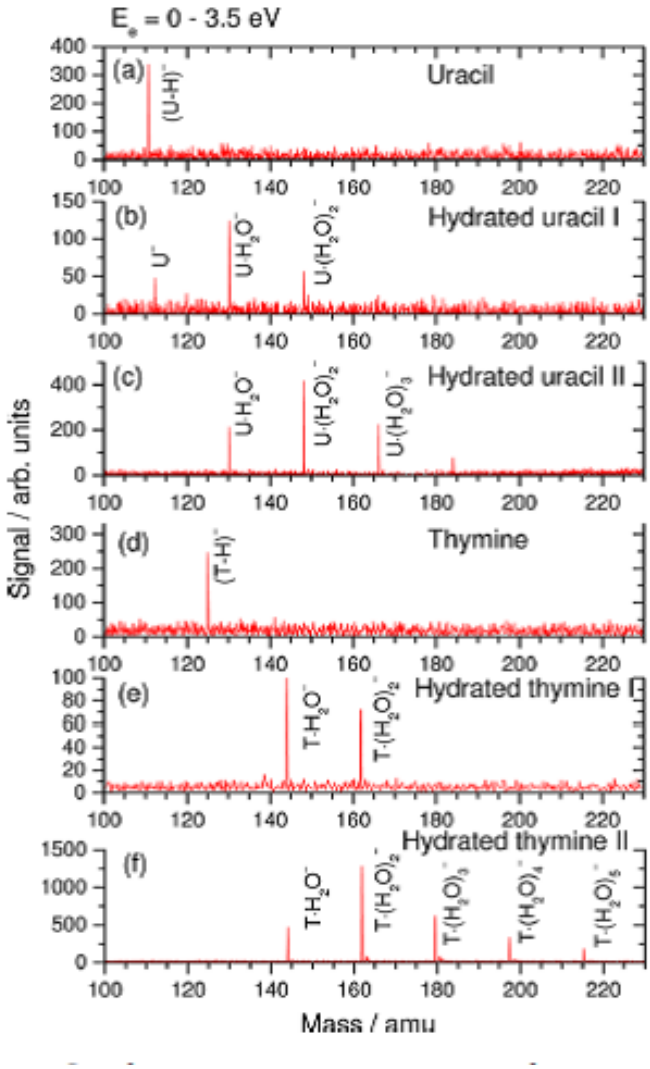

Figure 9. Cumulative negative ion mass spectra in the energy range from 0 to 3.5 eV for different targets: a and d, molecular beams of uracil and thymine without any humidification; b and e, minimal degree of microhydration in the beam; c and f) higher degree of microhydration. Reprinted with permission from Kočišek, Pysanenko, Fárník & Fedor (2016). Copyright 2016 American Chemical Society.

5. Applications

We now turn our attention to the use of the data and insight into electron scattering described in Sections 3 and 4.3 (Section 5.1.1). We also discuss calculations and experiments geared towards understanding radiosensitisers (Section 5.1.2). We then describe briefly other (non-medical) areas where electron scattering from biological molecules is relevant: biofules and electron transport linked to metabolical processes. Finally, we include a brief summary of the (very much related) research on positron scattering from biological molecules.

5.1. Biomedical applications

5.1.1. Track structure modelling Track structure simulations model the propagation of a radiation particle along a medium, its interactions with it, and the secondary particles that this interaction produces. One aim of such simulations is to determine dose (i.e., the amount of energy absorbed per unit volume) distribution. A number of packages exist (PARTRACK, PENELOPE, GEANT4, PTra, LEPTS, to name just a few) that can be used for this purpose. The simulations require as input integral and differential cross sections for all of the possible processes that can take place in the medium for a broad range of electron scattering energies.

Most of these simulations use water as a target (or a mix of simple molecules known as 'tissue equivalent material'). Some attempts have been made to understand the effect on energy deposition modelling of using, for example, pyrimidine data (Fuss, Ellis-Gibbings, Jones, Brunger, Blanco, Muoz, Limão-Vieira & García 2015). Very recently, the recommended gas-phase cross section data set of analogues of DNA constituents, i.e., pyrimidine, purine, THF, and trimethyl phosphate for electron scattering in the energy range between about 10 eV and 1 keV were reported (Bug et al. 2017). This data set includes a variety of cross sections: total scattering cross sections, differential and integral elastic scattering cross sections, double-differential, single-differential and total ionisation cross sections, total inelastic and total excitation cross sections. The data set can be used for track structure simulations of electrons with energies between about 30 eV and 1 keV (Bug et al. 2017). Although it is acknowledged that these cross sections will be significantly affected by the change of phase for lower energies ($\leq$ 30 eV) as shown for vibrational excitation cross sections for gas and condensed phases of pyrimidine in Figure 4, the data was implemented in track structure code system PTra (Bug, 2014) and could possibly be implemented in Geant4-DNA. The latter is an extension of the Geant4 toolkit for calculating initial radiation damage at the molecular level. We note than in Geant4-DNA physical processes (including elastic scattering, electronic excitation, vibrational excitation, ionisation and molecular attachment, and new models) were adapted to allow simulations of electrons with energies as low as 7.4 eV interacting with liquid water (Bernal et al. 2015). Finally, we also note that currently a development of simulation of track structures at low energy electrons for a mechanistic description not only of DNA damage but also repair has progressed extensively (Nikjoo, Taleei, Liamsuwan, Liljequist & Emfietzoglou 2016, Nikjoo, Emfietzoglou, Liamsuwan, Taleei, Liljequist & Uehara 2016).

5.1.2. Radiosensitisers and chemotheraphy drugs One of the important prerequisites for many radiosensitisers used in radiotherapy is a high DEA cross section. Since halogenated pyrimidines (mainly substituted uracil derivatives) have been shown to exhibit high sensitivity to electron attachment and a rich fragmentation pattern from DEA, they have attracted considerable interest as radiosensitisers. From a medical point of view, the substitution of pyrimidines in the genetic sequence of cellular

DNA does not affect gene expression. Several gas-phase experimental and theoretical studies of a variety of halogenated pyrimidines, such as 5-bromouracil (Abdoul-Carime et al. 2003, Abouaf et al. 2003*b*, Scheer et al. 2004, Abouaf & Dunet 2005, Denifl et al. 2005, Kossoski & Varella 2015), 5-chlorouracil (Abdoul-Carime et al. 2003, Denifl et al. 2003, Scheer et al. 2004, Denifl et al. 2004, Abouaf & Dunet 2005, Kossoski et al. 2014), 5-fluorouracil (Abdoul-Carime et al. 2003, Scheer et al. 2004, Abouaf & Dunet 2005, Kossoski et al. 2014), 5-iodouracil (Abdoul-Carime et al. 2003, Kossoski & Varella 2015), and 6-chlorouracil (Abouaf & Dunet 2005, Kossoski et al. 2014), have been performed. The experimental results indicate that the DEA cross sections are orders of magnitude higher than for the non-substituted precursors. The lowest π^* anion states of the halogenated pyrimidines follow similar pathways for fragmentation, primarily resulting in the formation of the halide anion. Moreover, the total anion yields for bromopyrimidine are much larger than for the chloro-derivatives; thus, bromopyrimidines indicate a greater potential as radiosensitisers in halogen-substituted DNA.

Gas-phase DEA studies have also been initiated on halogenated purines, such as chloroadenine (Kossoski et al. 2015), fluoroadenine (Rackwitz et al. 2016), and fluorinated nucleoside (2-deoxy-5-uorocytidine and 2,2-diuorocytidine (gemcitabine) Kopyra et al. 2014) to test their properties as potential radiosensitising drugs. Additionally, several studies of aromatic compounds containing nitro groups, e.g., 5-nitrouracil (Ptasińska et al. 2008, Abouaf et al. 2008), have been performed. The properties of 5-nitrouracil showed a radiosensitising nature similar to that of the halogenated pyrimidines, with the formation of a long-lived parent anion accompanied by multichannel fragmentation. Other nitro-containing molecules such as nitroimidazolic compounds have also been suggested for use in radiotherapy since LEEs can effectively induce their fragmentation (Tanzer, Feketeová, Puschnigg, Scheier, Illenberger & Denifl 2014, Tanzer et al. 2015) via DEA. This rich fragmentation pattern is totally quenched by the methylation of nitroimidazolic compounds below 2 eV. In contrast to halogenated and nitro group-containing drugs, DEA to hydroxyurea (a simple chemotherapeutic drug) led to the formation of NCO^- as the most dominant dissociation product. Its cross section was about 10 times higher than the other most abundant detected ions, i.e., $NCNH^-$ and $NHCONH_2^-$, which are both directly associated with the production of the biologically reactive OH species (Huber et al. 2016).

Common platinum-based drugs have been investigated in relation to concomitant treatment in which chemotherapeutic drugs and radiotherapy are combined. Both experiments (Kopyra et al. 2009) and calculations for electron scattering from cisplatin (a common chemotherapy drug) (Carey et al. 2013) have been performed that aim to explain how the complex that is responsible for inhibiting DNA replication is formed. One of the suggested mechanisms responsible for the observed synergy is the increase in the number of secondary reactive species induced by primary high-energy radiation in the close vicinity of the platinum compounds bounded to DNA. Indeed, the recent

gas-phase DEA studies of $PtBr_2$ demonstrated the formation of Br^- via two possible channels. These are: (1) the low-electron energy formation of both Br^- and PtBr ($\approx$1 eV) and (2) the formation of Br^-, and Pt and Br radicals that required higher-electron energies (Tanzer, Pelc, Huber, Śmiałek, Scheier, Probst & Denifl 2014). These experimental findings show that, for most studied radiosensitisers, highly reactive products are formed via DEA with high total cross sections, even close to 0 eV. This has significant implications for the further development of drug design for cancer treatment.

5.2. Biofuels

Biofuels are a renewable source of energy that has been given significant attention in recent years. One potential source is lignocellulosic biomass (made of cellulose, hemicellulose and lignin) from which ethanol can be obtained. The process requires the removal of lignin and hemicellulose and plasmas have been tested for this purpose. Calculations and experiments on electron scattering from these compounds (and the subunits that constitute them) have been performed to understand and inform the plasma treatment (Ridenti et al. 2016). Targets studied using the SMCPP method are: α-D-glucose β-D-glucose (da Costa et al. 2010), cellobiose (a glucose dimer) and β-D-xylose (de Oliveira et al. 2013), phenol, guaiacol, and *p*-coumaryl alcohol (de Oliveira et al. 2012). We note that electron scattering from phenol has been studied quite extensively, both experimentally and computationally (Neves, Jones, Lopes, Blanco, García, Ratnavelu & Brunger 2015, da Costa, de Oliveira, Bettega, do N. Varella, Jones, Brunger, Blanco, Colmenares, Limão-Vieira, García & Lima 2015, Neves, Jones, Lopes, Nixon, da Silva, Duque, de Oliveira, da Costa, do N. Varella, Bettega, Lima, Ratnavelu, García & Brunger 2015).

5.3. Electron transport and other metabolites

We briefly mention here experimental studies of resonance formation in various other biological molecules. ETS and DEA spectroscopy of plant hormones and their analogues have been performed to investigate their electron transfer behaviour and its link to respiration and photosynthesis (Pshenichnyuk & Modelli 2014). Herbicides (Scheer et al. 2014), ascorbic acid (electron exchange is thought to play a role in its cellular chemistry, Pshenichnyuk et al. 2016) and pesticides (Pshenichnyuk & Modelli 2013) where the products of DEA may be dangerous for mitochondrial functionalities as well as interfere with cellular signalling pathways, have also been studied with the same techniques.

Similarly, resonance formation in 1,4-benzoquinone has been studied theoretically (see references in Cheng & Huang 2014, Kunitsa & Bravaya 2016) and experimentally by ETS and EELS (Modelli & Burrow 1984, Allan 1983). Quinones are involved in biological electron transfer reactions like photosynthesis and some synthetic quinones are known for their antitumoral effect.

DEA experiments have been performed for biotin, a vitamin involved in the cellular response to DNA damage and other biological processes, both in the gas phase and in the condensed phase using DNA origami nanostructures (Keller et al. 2013).

5.4. Positron scattering

The study of positron collisions with biologically relevant molecules has been stimulated by the medical uses of positrons, in particular positron emission tomography (PET). All the processes induced by electron scattering are also induced by positrons, although not DEA. However, additional processes are possible: positronium formation and the annihilation of the positron with an electron leading to the emission of gamma photons (the process PET is based on).

From a theoretical perspective, below the positronium formation threshold (determined by the difference between the molecule's ionisation potential and the ground state energy of positronium), the same methods can be used to study positron and electron scattering. Exchange is no longer present, so more care needs to be taken to describe polarization effects accurately. Above the threshold, however, positron formation cross sections grow rapidly and the exclusion of this channel from the calculations can affect the accuracy of the results. This threshold can be very low for biomolecules, as the first electron excitation threshold tends to be low. Inclusion of positronium formation in theoretical low energy scattering studies remains a challenge. From an experimental perspective, the main additional difficulty is the generation of a sufficiently intense positron beam. We refer the reader to a few reviews (Surko et al. 2005, Gribakin et al. 2010, Danielson et al. 2015) that summarise the techniques and methods applied.

The amount of cross section data for positron scattering is significantly smaller than that for electrons. We highlight a number of recent works: elastic scattering from uracil was studied theoretically (Franz et al. 2014) and total cross sections were determined experimentally (Surdutovich et al. 2008, Anderson et al. 2014). ECS for other DNA bases have also been calculated (Franz & Gianturco 2014) (the same issues regarding the effect of a large dipole moment affect the determination of elastic cross sections in positron scattering). Total, elastic, and inelastic cross sections for collisions with THF have been determined theoretically (using the IAM-SCAR method) and experimentally over a range of higher energies (Chiari, Anderson, Tattersall, Machacek, Palihawadana, Makochekanwa, Sullivan, García, Blanco, McEachran, Brunger & Buckman 2013) as have those of 3-hydroxy-tetrahydrofuran (Chiari, Palihawadana, Machacek, Makochekanwa, García, Blanco, Brunger, Buckman & Sullivan 2013). ECS and DCS for THF have also been determined theoretically (Franz & Gianturco 2013). Experimental total and positronium formation cross sections for scattering from pyrimidine as well as theoretical ECS and DCS have been determined (Palihawadana et al. 2013, Sanz et al. 2013, Barbosa et al. 2015). Finally, ECS have been determined for scattering from glycine and alanine (Nunes et al. 2016).

6. Latest developments and outlook

We finalize this Topical Review by highlighting some recent technical and methodological developments and indicating what other ones may be needed. We also summarise current and future data requirements.

6.1. Experimental developments

Velocity map imaging In order to study the dynamics of electron induced dissociation, velocity map imaging (VMI) of fragment ions from DEA was developed a decade ago (Nandi et al. 2005, Nandi et al. 2006). Since then, several theoretical and experimental results relevant to DEA studied by momentum imaging have been obtained and surveyed in a recent review article (Slaughter et al. 2016). While a significant amount of details about chemical dynamics was revealed for small polyatomic systems, the only study relevant to biological molecules was reported for uracil (Kawarai et al. 2014). There are a couple of significant challenges for VMI in the case of relatively large and complex biomolecules: the detection of a single fragment and misidentification of fragments since most of the excess energy is transferred into internal degrees of freedom in the form of rotational and vibrational excitation, and/or conformational changes (e,g., automerisation) (Slaughter et al. 2016). In the case of uracil, the momentum imaging study revealed dynamical information for resonances at ∼6 eV with several possible dissociation pathways (Kawarai et al. 2014); Figure 10 presents the ion momentum distribution of H^-. We note that Kawarai et al. (2014) based the theoretical interpretation of these results on the existence of a Feshbach resonance of A″ symmetry that has not been identified by the most sophisticated *ab initio* calculations (Mašín & Gorfinkiel 2014). In addition to dissociation pathways observed in standard DEA studies, a new decay channel was also suggested that exhibiting much faster decay than the intermediate dehydrogenated anion of nucleobases, which is shown for thymine in Figure 7.

A number of groups in Europe, Asia and the United States have well established experimental setups to perform these types of measurements. Further development and use of this technique for more complex systems will lead to predictions of dissociation dynamics and to advancing the understanding of the DEA process to isolated biomolecules as well as aggregates (e.g., clusters).

Characterisation of neutral radicals from a DEA process In all previous DEA studies, only negatively-charged fragments were detected, while neutral fragments were unidentified. Neutral-fragment detection is important to complete the description of reaction pathways induced by low-energy electrons. In addition, the neutrals produced are radicals that exhibit high reactivity in a cellular medium. To narrow this gap, there is an urgent need for experimental approaches to detect neutral species formed due to DEA to biomolecules. Until recently, technical challenges hindered the ability to address neutral detection. Previous conclusions regarding neutral products were often deduced from experimental results supported by calculating which fragmentation pathways were

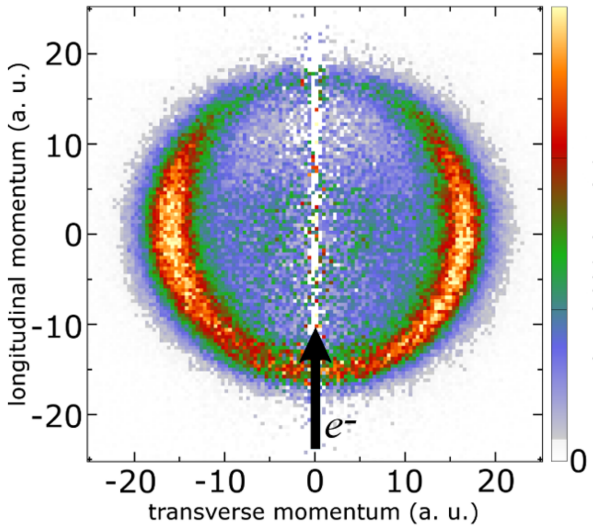

Figure 10. Ion momentum distribution of H^-, measured in atomic units (a. u.), that results from DEA to uracil at an electron beam energy of 6 eV. The electron beam direction is indicated by an arrow. The image shows that H^- is ejected preferentially in the perpendicular or backward directions with respect to the electron beam. Reprinted with permission from Kawarai et al. (2014). Copyright 2014 American Chemical Society.

the most energetically favorable. This was determined from the reaction enthalpies for production of both anions, which were observed by mass spectrometry, and possible neutral products, which would assist dissociation. However, this type of theoretical approach does not include formation of TNIs.

The challenges of detecting neutrals from DEA have been overcome by developing a novel two-step electron ionisation technique, which will significantly enhance our understanding of DEA processes. This technique was used, for the first time, for the measurement and characterisation of neutrals from DEA to carbon tetrachloride (CCl_4) (Li et al. 2017). CCl_4 was chosen due to its high DEA cross section at the electron energy of 0 eV. No such investigations have been performed for biomolecules. Information about neutrals can greatly change current understanding of DEA to simple biomolecules (units of DNA and proteins) and carries the promise to be translated to more complex systems in the condensed phase and more realistic conditions: the possibility of identifying these neutrals will lead to establishing a comprehensive understanding of DNA and cell-damage mechanisms.

Cluster selectivity The experiments described in Section 4.2 involve scattering from a gas containing a range of clusters: the size and composition of these can only be partially controlled. Performing experiments with selected clusters (i.e., those containing a specific number of molecules) would simplify their interpretation as well as facilitate the comparison with theoretical results. Encouraging work is being performed to setup an electron attachment experiment with Stark selected clusters (Ryszka et al. 2015).

6.2. Theoretical developments

An improved description of the effect of electron scattering on biomolecules and their clusters requires two ingredients:

- highly efficient software that enables the study of larger targets with increased accuracy. Indeed, the study of electron collisions with biological targets has been one of the main drivers of various software developments carried out over the last decade or so (e.g., of the R-matrix software, see Carr et al. 2012). Calculations are still pushing at the limit of what current codes can do, in particular when it comes to aggregates and even for isolated molecules when describing processes involving electronic excitation and core-excited resonances. Improving and optimizing the description of the electronically excited states of the target in the scattering software would also be of benefit.
- methodological developments that will improve our ability to describe some of the processes taking place. Here, for example, we highlight the need for techniques to describe DEA when several nuclear degrees of freedom are important and interpret velocity map imaging results beyond the fairly restricting axial recoil approximation (more sophisticated approaches are available but have not been applied to biomolecules, in part due to the need to calculate resonance data as a function of all nuclear coordinates, see Slaughter et al. 2016). Approaches to treat big(ger) clusters, perhaps based on multiple-scattering as used for pure water clusters (Caprasecca et al. 2009), would also be benefitial.

The application of adapted quantum chemistry techniques to the description of resonances described in Section 3.4.1 may also provide useful information for the modelling and understanding of DEA.

It is worth mentioning that another push towards better computational description of electron-biomolecule interactions comes from the study of molecular processes induced by ultrashort laser pulses (e.g., high-harmonic generation in biomolecules (Marangos 2016), charge migration (Calegari et al. 2016)). Many of the theoretical approaches currently used to describe these processes in organic and biomolecules are highly simplified (i.e., single active electron). However, (multi)electron correlation, far more significant for these molecules than for atoms, plays an important role in these processes. The provision of accurate photoionisation data (that involves determining similar quantities to those needed in electron scattering studies and therefore can be done using the same software) is an essential step to improve the computational description of the effects induced by the laser field. We note also that the use of ultrashort pulses is enabling the study of excited state relaxation dynamics (e.g., of pyrimidine nucleosides and radiosensiziters), electron transfer in photosynthetic molecules and other processes of biological relevance that are also linked to electron scattering (see papers that follow Minns & Kirrander 2016).

6.3. Data requirements

A complete electron scattering cross section database for biomolecules could be employed to model radiation interactions with biological matter and advance our understanding in many scientific areas including radiotherapy, diagnostics, and medical imaging (Section 5.1.1), plasmas used in medicine (Samukawa et al. 2012) and in the treatment of biomass (Section 5.2) as well as astrophysics (Dubernet et al. 2016), particularly for formation of biomolecules.

Recent work using a mixture of water and pyrimidine data in the LEPTS modelling suite has suggested the use of only water might not provide a quantitatively correct description of the macroscopic effects of radiation in biological material (Fuss, Ellis-Gibbings, Jones, Brunger, Blanco, Muñoz, Limão-Vieira & García 2015). Unfortunately, the cross section data sets required for this type of track structure modelling remain incomplete (Bug et al. 2017). Accurate and self-consistent data for a wide range of processes and a variety of targets is needed. This includes not only the processes discussed in this Topical Review, but others too. For example, electron emission cross sections for high-energy particle impact are required as input for simulations in the Bragg peak region (Rudek et al. 2016). The effects of the condensed environment in the cross sections is likely to be important but not yet fully explored. A detailed understanding of the DEA process, for cell constituents, radiosensitisers, etc., is also crucial.

Collisions of low-energy electrons with excited biomolecules can play an important role in living systems since radiation can induce molecular excitation while secondary electrons produced in large quantities in the cellular system can interact with these excited targets. Many studies of DEA to biomolecules at elevated temperatures showed a so-called hot band transition at 0 eV, which was attributed to thermally excited rotational and vibrational modes, as seen in Figure 6. Electron impact cross sections, including elastic and inelastic processes, for the vibrationally and electronically excited molecules differ both in order of magnitude and/or the energetics for the formation of resonances from those for molecules in the ground state (Yoon et al. 2014). Thus, determining electron impact cross sections for excited targets is important for radiation therapy research and other fields. A recent review discussed the need for more data and evaluated the cross sections available in literature for different processes (dissociation, ionisation and the attachment) for a few simple excited molecules such as H_2, D_2, T_2, HD, HT, DT, N_2, O_2, and CO_2 (Yoon et al. 2014). The data available is still extremely limited, especially for larger compounds such as biomolecules.

New approaches to the use of radiation may require further information on electron induced processes. For example, the recent development of one-atom-thick films of a radioactive isotope (Pronschinske et al. 2015) has brought about the prospect of coated nanoparticles being injected directly into tumours as a highly efficient source of highly localised low-energy electrons (Sanche 2015). The modelling of the induced radiation damage may require cross sections for new targets.

Finally, we mention that a handful of databases are being established

that include data of electron-molecule scattering cross sections: the Belgrade electron/atom(molecule) database BEAMDB (http://servo.aob.rs/emol/)(Marinković et al. 2015), Innsbruck's IDEADB for DEA spectra (http://ideadb.uibk.ac.at) (Denifl et al. 2013), etc. VAMDC (http://portal.vamdc.org/vamdc_portal/home.seam) and RADAM (http://mbnresearch.com) act as portals to many atomic and molecular databases; although not specifically about biologically relevant targets, some information about these type of gas-phase targets is available (particularly in the DEA database). These databases collect, evaluate, and disseminate reliable cross section data. The task is not a trivial one: incorporating reliable values in the databases requires a critical compilation of available data, both experimental and theoretical: few quantitative comparisons of this data have been performed in the literature, where in many cases the results are just presented in graphical form. In addition, many of the cross sections published (including the vast majority of theoretical ones) do not come accompanied by uncertainty bars.

Acknowledgements

S.P. acknowledges the U.S. Department of Energy Office of Science, Office of Basic Energy Sciences under Award Number DE-FC02-04ER15533 (NDRL no: 5167)

References

Abdoul-Carime H, Gohlke S & Illenberger E 2004*a* *Phys. Rev. Lett.* **92**(16), 168103.
Abdoul-Carime H, Gohlke S & Illenberger E 2004*b* *Phys. Chem. Chem. Phys.* **6**, 161–164.
Abdoul-Carime H, Gohlke S & Illenberger E 2005 *Chem. Phys. Lett.* **402**(46), 497 – 502.
Abdoul-Carime H, Huels M A, Illenberger E & Sanche L 2003 *Int. J. Mass Spectrom.* **228**(23), 703 – 716.
Abdoul-Carime H & Illenberger E 2004 *Chem. Phys. Lett.* **397**(46), 309 – 313.
Abdoul-Carime H, König-Lehmann C, Kopyra J, Farizon B, Farizon M & Illenberger E 2009 *Chem. Phys. Lett.* **477**(46), 245 – 248.
Abouaf R 2008 *Chem. Phys. Lett.* **451**(13), 25 – 30.
Abouaf R & Dunet H 2005 *Eur. Phys. J. D* **35**(2), 405–410.
Abouaf R, Pommier J & Dunet H 2003*a* *Chem. Phys. Lett.* **381**(34), 486 – 494.
Abouaf R, Pommier J & Dunet H 2003*b* *Int. J. Mass Spectrom.* **226**(3), 397 – 403.
Abouaf R, Pommier J, Dunet H, Quan P, Nam P C & Nguyen M T 2004 *J. Chem. Phys.* **121**(23), 11668–11674.
Abouaf R, Ptasinska S & Teillet-Billy D 2008 *Chem. Phys. Lett.* **455**(46), 169 – 173.
Aflatooni K, Gallup G & Burrow P 1998 *Journal of Physical Chemistry A* **102**(31), 6205–6207.
Aflatooni K, Hitt B, Gallup G A & Burrow P D 2001 *J. Chem. Phys.* **115**(14), 6489–6494.
Aflatooni K, Scheer A M & Burrow P D 2006 *J. Chem. Phys.* **125**, 054301.
Alizadeh E, Gschliesser D, Bartl P, Hager M, Edtbauer A, Vizcaino V, Mauracher A, Probst M, Mrk T D, Ptasińska S, Mason N J, Denifl S & Scheier P 2011 *J. Chem. Phys.* **134**(5), 054305.
Alizadeh E, Orlando T M & Sanche L 2015 *Ann. Rev. Phys. Chem.* **66**(1), 379–398.
Alizadeh E & Sanche L 2012 *Chemical Reviews* **112**(11), 5578–5602.
Allan M 1983 *Chemical Physics* **81**, 235.
Allan M 2007*a* *Phys. Rev. Lett.* **98**, 123201.
Allan M 2007*b* *J. Phys. B* **40**(17), 3531.

Allan M 2012 *J. Phys.: Conf. Ser.* **388**(1), 012001.
Allan M, Regeta K, Gorfinkiel J D, Mašín Z, Grimme S & Bannwarth C 2016 *Eur. Phys. J. D* **70**(5), 123.
Anderson E K, Boadle R A, Machacek J R, Chiari L, Makochekanwa C, Buckman S J, Brunger M J, García G, Blanco F, Ingolfsson O & Sullivan J P 2014 *J. Chem. Phys.* **141**(3), 034306.
Anzai K, Kato H, Hoshino M, Tanaka H, Itikawa Y, Campbell L, Brunger M, Buckman S, Cho H, Blanco F, García G, Limão-Vieira P & Inglfsson O 2012 *Eur. Phys. J. D* **66**(2), 36.
Aronova M & Leapman R 2012 *MRS Bulletin* **37**(1), 53–62.
Asfandiarov N L, Pshenichnyuk S A, Vorob'ev A S, Nafikova E P, Elkin Y N, Pelageev D N, Koltsova E A & Modelli A 2014 *Rapid Commun. Mass Spectrom.* **28**(14), 1580–1590.
Baccarelli I, Bald I, Gianturco F A, Illenberger E & Kopyra J 2011 *Phys. Rep.* **508**(1-2), 1–44.
Baccarelli I, Gianturco F A, Grandi A, Sanna N, Lucchese R R, Bald I, Kopyra J & Illenber E 2007 *J. Am. Chem. Soc.* **129**(19), 6269–6277.
Baccarelli I, Sebastianelli F, Gianturco F A & Sanna N 2009 *Eur. Phys. J. D* **51**(1), 131 – 136.
Bald I, Čurík R, Kopyra J & Tarana M 2017 *in* A. V Solov'yov, ed., 'Nanoscale Insights into Ion-Beam Cancer Therapy' Springer International Publishing Cham pp. 159–207.
Barbosa A S & Bettega M H F 2013 *J. Chem. Phys.* **139**(21), 214301.
Barbosa A S, Pastega D F & Bettega M H F 2015 *J. Chem. Phys.* **143**(24), 244316.
Baskar R & Itahana K 2017 *Int. J. Med. Sci.* **14**(1), 13.
Bellert D, Burns K L, Van-Oanh N T, Wang J & Breckenridge W 2003 *Chem. Phys. Lett.* **381**(34), 381 – 384.
Bernal M, Bordage M, Brown J, Davdkov M, Delage E, Bitar Z E, Enger S, Francis Z, Guatelli S, Ivanchenko V, Karamitros M, Kyriakou I, Maigne L, Meylan S, Murakami K, Okada S, Payno H, Perrot Y, Petrovic I, Pham Q, Ristic-Fira A, Sasaki T, tpn V, Tran H, Villagrasa C & Incerti S 2015 *Physica Medica* **31**(8), 861 – 874.
Blanco F & García G 2002 *Physics Letters A* **295**(4), 178 – 184.
Blanco F & García G 2003 *Phys. Rev. A* **67**, 022701.
Bouchiha D, Gorfinkiel J D, Caron L G & Sanche L 2006 *J. Phys. B: At. Mol. Opt. Phys.* **39**, 975–986.
Boudaïffa B, Cloutier P, Hunting D, Huels M A & Sanche L 2000 *Science* **287**, 1658–1660.
Brunger M J, Ratnavelu K, Buckman S J, Jones D B, Muñoz A, Blanco F & García G 2016 *Eur. Phys. J. D.* **70**(3), 46.
Bug M U, Baek W Y, Rabus H, Villagrasa C, Meylan S & Rosenfeld A B 2017 *Rad. Phys. Chem.* **130**, 459 – 479.
Burean E, Abouaf R, Lafosse A, Azria R & Swiderek P 2008 *J. Phys. Chem. C* **112**(25), 9405–9411.
Burke P G 2011 *R-Matrix Theory of Atomic Collisions: Application to Atomic, Molecular and Optical Processes* Springer.
Burrow P D, Gallup G A & Modelli A 2008 *J. Phys. Chem. A* **112**(17), 4106–4113.
Calegari F, Trabattoni A, Palacios A, Ayuso D, Castrovilli M C, Greenwood J B, Decleva P, Martn F & Nisoli M 2016 *J. Phys. B* **49**(14), 142001.
Caprasecca S, Gorfinkiel J D, Bouchiha D & Caron L G 2009 *J. Phys. B: At. Mol. Opt. Phys.* **42**, 095205.
Carelli F & Gianturco F A 2016 *The European Physical Journal D* **70**(6), 145.
Carey R, Lucchese R R & Gianturco F A 2013 *J. Chem. Phys.* **138**(20), 204308.
Caron L, Sanche L, Tonzani S & Greene C H 2008 *Phys. Rev. A* **78**, 042710.
Caron L, Sanche L, Tonzani S & Greene C H 2009 *Phys. Rev. A* **80**, 012705.
Carr J M, Galiatsatos P G, Gorfinkiel J D, Harvey A G, Lysaght M A, Madden D, Mašín Z, Plummer M, Tennyson J & Varambhia H N 2012 *Eur. Phys. J. D* **66**(3), 58.
Cheng H & Huang Y 2014 *Phys. Chem. Chem. Phys.* **16**, 26306.
Cheng H Y, Chen Y C, Lin C J, Liu W C & Hsieh S H 2016 *Computational and Theoretical Chemistry* **1075**, 18–29.
Chernyshova I, Kontros J, Markush P & Shpenik O 2012 *Optics and Spectroscopy* **113**(1), 5–8.
Chernyshova I V, Kontros E J, Markush P P & Shpenik O B 2013 *Optics and Spectroscopy* **115**(5), 645–650.

Chiari L, Anderson E, Tattersall W, Machacek J R, Palihawadana P, Makochekanwa C, Sullivan J P, García G, Blanco F, McEachran R P, Brunger M J & Buckman S J 2013 *J. Chem. Phys.* **138**(7), 074301.

Chiari L, Palihawadana P, Machacek J R, Makochekanwa C, García G, Blanco, F.and McEachran R P, Brunger M J, Buckman S J & Sullivan J P 2013 *J. Chem. Phys.* **138**, 074302.

Colyer C J, Bellm S M, Blanco F, García G & Lohmann B 2011 *J. Phys.: Conf. Ser.* **288**(1), 012014.

Colyer C J, Vizcaino V, Sullivan J P, Brunger M J & Buckman S J 2007 *New J. Phys.* **9**(2), 41.

da Costa R F, Bettega M H F & Lima M A P 2008*a* *Phys. Rev. A* **77**, 012717.

da Costa R F, Bettega M H F & Lima M A P 2008*b* *Phys. Rev. A* **77**, 042723.

da Costa R F, Bettega M H F, Varella M T d N & Lima M A P 2010 *J. Chem. Phys.* **132**(12), 124309.

da Costa R F, da Paixo F J & Lima M A P 2005 *J. Phys. B* **38**(24), 4363.

da Costa R F, de Oliveira E M, Bettega M H F, do N. Varella M T, Jones D B, Brunger M J, Blanco F, Colmenares R, Limão-Vieira P, García G & Lima M A P 2015 *J. Chem. Phys.* **142**(10), 104304.

da Costa R F, Varella M T d N, Bettega M H F & Lima M A P 2015 *Eur. Phys. J. D* **69**(6), 159.

da Silva F F, Denifl S, Maerk T D, Ellis A M & Scheier P 2010 *J. Chem. Phys.* **132**(21), 214306.

Dampc M, Milosavljević A R, Linert I, Marinković B P & Zubek M 2007 *Phys. Rev. A* **75**, 042710.

Danielson J R, Dubin D H E, Greaves R G & Surko C M 2015 *Rev. Mod. Phys.* **87**, 247–306.

Dawley M M & Ptasińska S 2014 *Int. J. Mass Spectrom.* **365-366**, 143 – 151.

Dawley M M, Tanzer K, Carmichael I, Denifl S & Ptasińska S 2015 *J. Chem. Phys.* **142**(21), 215101.

de Oliveira E M, da Costa R F, Sanchez S d, Natalense A P P, Bettega M H F, Lima M A P & Varella M T d N 2013 *Phys. Chem. Chem. Phys.* **15**, 1682–1689.

de Oliveira E M, d'A. Sanchez S, Bettega M H F, Natalense A P P, Lima M A P & Varella M T d N 2012 *Phys. Rev. A* **86**, 020701.

Denifl S, Candori P, Ptasińska S, Limão-Vieira P, Grill V, Märk T D & Scheier P 2005 *Eur. Phys. J. D* **35**(2), 391–398.

Denifl S, Flosadóttir H D, Edtbauer A, Ingólfsson O, Märk T D & Scheier P 2010 *Eur. Phys. J. D.* **60**(1), 37–44.

Denifl S, García G, Huber B A, Marinković B P, Mason N, Postler J, Rabus H, Rixon G, Solov'yov A V, Suraud E & Yakubovich A V 2013 *J. Phys.: Conf. Ser.* **438**(1), 012016.

Denifl S, Matejčík S, Gstir B, Hanel G, Probst M, Scheier P & Märk T D 2003 *J. Chem. Phys.* **118**(9), 4107–4114.

Denifl S, Matejčík S, Ptasinska S, Gstir B, Probst M, Scheier P, Illenberger E & Märk T D 2004 *J. Chem. Phys.* **120**(2), 704–709.

Denifl S, Sulzer P, Huber D, Zappa F, Probst M, Märk T, Scheier P, Injan N, Limtrakul J, Abouaf R & Dunet H 2007 *Angew. Chem., Int. Ed.* **46**(27), 5238–5241.

Dillon M A, Tanaka H & Spence D 1989 *Radiation Research* **117**(1), 1.

Do T P T, Duque H V, Lopes M C A, Konovalov D A, White R D, Brunger M J & Jones D B 2015 *J. Chem. Phys.* **142**(12), 124306.

Do T P T, Leung M, Fuss M, García G, Blanco F, Ratnavelu K & Brunger M J 2011 *J. Chem. Phys.* **134**(14), 144302.

Domcke W 1991 *Phys. Rep.* **208**(2), 97–188.

Dora A, Bryjko L, van Mourik T & Tennyson J 2012*a* *J. Chem. Phys.* **136**(2), 024324.

Dora A, Bryjko L, van Mourik T & Tennyson J 2012*b* *J. Phys. B: At. Mol. Opt. Phys.* **45**(17), 175203.

Dora A, Tennyson J, Bryjko L & van Mourik T 2009 *J. Chem. Phys.* **130**, 164307.

dos Santos J S, da Costa R F & Varella M T d N 2012 *J. Chem. Phys.* **136**(8), 084307.

Dubernet M L, Antony B K, Ba Y A, Babikov Y L, Bartschat K, Boudon V, Braams B J, Chung H K, Daniel F, Delahaye F, Zanna G D, de Urquijo J, Dimitrijevi M S, Domaracka A, Doronin M, Drouin B J, Endres C P, Fazliev A Z, Gagarin S V, Gordon I E, Gratier P, Heiter U, Hill C, Jevremovi D, Joblin C, Kasprzak A, Krishnakumar E, Leto G, Loboda P A, Louge T, Maclot S, Marinković B P, Markwick A, Marquart T, Mason H E, Mason N J, Mendoza C, Mihajlov A A, Millar T J, Moreau N, Mulas G, Pakhomov Y, Palmeri P, Pancheshnyi S, Perevalov V I,

Piskunov N, Postler J, Quinet P, Quintas-Snchez E, Ralchenko Y, Rhee Y J, Rixon G, Rothman L S, Roueff E, Ryabchikova T, Sahal-Brchot S, Scheier P, Schlemmer S, Schmitt B, Stempels E, Tashkun S, Tennyson J, Tyuterev V G, Vujić V, Wakelam V, Walton N A, Zatsarinny O, Zeippen C J & Zwölf C M 2016 *J. Phys. B* **49**(7), 074003.

Duque H V, Do T P T, Lopes M C A, Konovalov D A, White R D, Brunger M J & Jones D B 2015 *J. Chem. Phys.* **142**(12), 124307.

Fabrikant I I 1991 *Phys. Rev. A* **43**, 3478–3486.

Fabrikant I I 2016 *J. Phys. B* **49**(22), 222005.

Fabrikant I I, Eden S, Mason N J & Fedor J 2017 *in* C. C. L Ennio Arimondo & S. F Yelin, eds, 'Advances In Atomic, Molecular, and Optical Physics' Vol. 66 of *Advances In Atomic, Molecular, and Optical Physics* Academic Press pp. 545 – 657.

Feketeová L & O'Hair R A J 2009 *Rapid Commun. Mass Spectrom.* **23**(20), 3259–3263.

Ferlay J, Soerjomataram I, M. Ervik R D, S. Eser C M, Rebelo M, Parkin D M, Forman D & Bray F 2013 'Globocan 2012 v1.0, cancer incidence and mortality worldwide: Iarc cancerbase no. 11 [internet]. lyon, france: International agency for research on cancer'.
URL: *http://globocan.iarc.fr*

Ferraz J R, dos Santos A S, de Souza G L C, Zanelato A I, Alves T R M, Lee M T, Brescansin L M, Lucchese R R & Machado L E 2013 *Phys. Rev. A* **87**, 032717.

Flosadóttir H, Denifl S, Zappa F, Wendt N, Mauracher A, Bacher A, Jónsson H, Märk T, Scheier P & Ingólfsson O 2007 *Angew. Chem., Int. Ed.* **46**(42), 8057–8059.

Franz J & Gianturco F A 2013 *J. Chem. Phys.* **139**(20), 204309.

Franz J & Gianturco F A 2014 *Eur. Phys. J. D.* **68**(10), 279.

Franz J, Gianturco F & Baccarelli I 2014 *Eur. Phys. J. D* **68**(7), 183.

Freitas T C, Coutinho K, Varella M, Lima M A P & Canuto S 2013 *J. Chem. Phys.* **138**, 174307.

Freitas T C, d'A. Sanchez S, Varella M T d N & Bettega M H F 2011 *Phys. Rev. A* **84**, 062714.

Freitas T C, Lima M A P, Canuto S & Bettega M H F 2009 *Phys. Rev. A* **80**(6), 062710.

Fröstel M, Neustetter M, Denifl S, Lelievre F & Hergenhahn U 2015 *Rev. Sci. Instrum.* **86**(7), 073103.

Fujimoto M M, de Lima E V R & Tennyson J 2016 *J. Phys. B* **49**(21), 215201.

Fujimoto M M, Tennyson J & Michelin S E 2014 *Eur. Phys. J. D* **68**(3), 67.

Fujita T, Kondo M & Takayanagi T 2016 *Computational and Theoretical Chemistry* **1075**, 70 – 76.

Fuss M C, Ellis-Gibbings L, Jones D B, Brunger M J, Blanco F, Muñoz A, Limão-Vieira P & García G 2015 *J. Appl. Phys.* **117**(21), 214701.

Fuss M C, Sanz A G, Blanco F, Limão-Vieira P, Brunger M J & García G 2014 *Eur. Phys. J. D* **68**(6), 1–8.

Fuss M, Ellis-Gibbings L, Jones D, Brunger M, Blanco F, Muoz A, Limão-Vieira P & García G 2015 *J. Appl. Phys.* **117**(21), 214701.

Galasso V, Kova B & Modelli A 2007 *Chem. Phys.* **335**(23), 141 – 154.

Gallup G A, Burrow P D & Fabrikant I I 2009 *Phys. Rev. A* **79**(4), 042701.

Gallup G A & Fabrikant I I 2011 *Phys. Rev. A* **83**(1), 012706.

Gauf A, Hargreaves L R, Jo A, Tanner J, Khakoo M A, Walls T, Winstead C & McKoy V 2012 *Phys. Rev. A* **85**, 052717.

Geddes S, Zahardis J, Eisenhauer J & Petrucci G A 2009 *Int. J. Mass Spectrom.* **282**(12), 13.

Gianturco F A & Jain A 1986 *Phys. Rep.* **143**(6), 347–425.

Gianturco F A, Lucchese R R, Langer J, Martin I, Stano M, Karwasz G & Illenberger E 2005 *Eur. Phys. J. D* **35**, 417–428.

Gianturco F A, Lucchese R R & Sanna N 1994 *J. Chem. Phys.* **100**(9), 6464–6471.

Gianturco F A, Sebastianelli F, Lucchese R R, Baccarelli I & Sanna N 2008 *J. Chem. Phys.* **128**(17), 174302.

Gianturco F A, Sebastianelli F, Lucchese R R, Baccarelli I & Sanna N 2009 *J. Chem. Phys.* **131**(24), 249901.

Gianturco F, Thompson D & Jain A 1995 *in* W. M Huo & F. A Gianturco, eds, 'Computational

Methods for Electron-Molecule Collisions' Springer US pp. 75–118.
Gohlke S, Rosa A, Illenberger E, Brning F & Huels M A 2002 *J. Chem. Phys.* **116**(23), 10164–10169.
Gorfinkiel J D & Caprasecca S 2012 *in* G García Gomez-Tejedor & M. C Fuss, eds, 'in Radiation Damage in Biomolecular Systems' Springer Netherlands pp. 127–142.
Gribakin G F, Young J A & Surko C M 2010 *Rev. Mod. Phys.* **82**, 2557–2607.
Gschliesser D, Vizcaino V, Probst M, Scheier P & Denifl S 2012 *Chemistry A European Journal* **18**(15), 4613–4619.
Hall E & Giaccia A 2012 *Radiobiology for the Radiologist* Wolters Kluwer Health.
Hamann T, Edtbauer A, Ferreira da Silva F, Denifl S, Scheier P & Swiderek P 2011 *Phys. Chem. Chem. Phys.* **13**, 12305–12313.
Hargreaves L R, Albaridy R, Serna G, Lopes M C A & Khakoo M A 2011 *Phys. Rev. A* **84**, 062705.
Herbert J M 2015 *in* Parrill, AL and Lipkowitz, KB, ed., 'Rev. Comp. Ch.' Vol. 28 Wiley pp. 391–517.
Huber S E, Śmiałek M A, Tanzer K & Denifl S 2016 *J. Chem. Phys.* **144**(22), 224309.
Huo W M & Gianturco F A, eds 1995 *Computational Methods for Electron Molecule Collisions* Plenum Press, New York.
Itikawa Y & Mason N 2005 *J. Phys. Chem. Ref. Data* **34**, 1–22.
Janečková R, Kubala D, May O, Fedor J & Allan M 2013 *Phys. Rev. Lett.* **111**, 213201.
Jensen F 1999 *Introduction to Computational Chemistry* Wiley Chircester.
Jones D B, Ellis-Gibbings L, García G, Nixon K L, Lopes M C A & Brunger M J 2015 *J. Chem. Phys.* **143**(9), 094304.
Kanazawa Y, Ehara M & Sommerfeld T 2016 *J. Phys. Chem. A* **120**(9), 1545–1553.
Kawarai Y, Weber T, Azuma Y, Winstead C, McKoy V, Belkacem A & Slaughter D S 2014 *J. Phys. Chem. Lett.* **5**(21), 3854–3858.
Keller A, Kopyra J, Gothelf K V & Bald I 2013 *New J. Phys.* **15**(8), 083045.
Keller A, Rackwitz J, Cauet E, Lievin J, Koerzdoerfer T, Rotaru A, Gothelf K V, Besenbacher F & Bald I 2014 *Sci. Rep.* **4**, 7391.
Keolopile Z G, Gutowski M, Buonaugurio A, Collins E, Zhang X, Erb J, Lectka T, Bowen K H & Allan M 2015 *J. Am. Chem. Soc.* **137**(45), 14329–14340.
König C, Kopyra J, Bald I & Illenberger E 2006 *Phys. Rev. Lett.* **97**(1), 018105.
Kopyra J 2012*a* *Chem. Phys. Lett.* **533**, 87 – 91.
Kopyra J 2012*b* *Phys. Chem. Chem. Phys.* **14**, 8287–8289.
Kopyra J & Abdoul-Carime H 2015 *J. Chem. Phys.* **142**(17), 174303.
Kopyra J, Keller A & Bald I 2014 *RSC Adv.* **4**, 6825–6829.
Kopyra J, König-Lehmann C, Bald I & Illenberger E 2009 *Angew. Chem., Int. Ed.* **48**(42), 7904–7907.
Kopyra J, König-Lehmann C & Illenberger E 2012 *Chem. Phys. Lett.* **550**, 47 – 51.
Kopyra J, König-Lehmann C & Illenberger E 2013 *Chem. Phys. Lett.* **578**, 54 – 58.
Kopyra J, Szamrej I, Abdoul-Carime H, Farizon B & Farizon M 2012 *Phys. Chem. Chem. Phys.* **14**, 8000–8004.
Kossoski F, Bettega M H F & Varella M T d N 2014 *J. Chem. Phys.* **140**(2), 024317.
Kossoski F, Kopyra J & Varella M T d N 2015 *Phys. Chem. Chem. Phys.* **17**(43), 28958–28965.
Kossoski F & Varella M T d N 2015 *Phys. Chem. Chem. Phys.* **17**, 17271–17278.
Kočišek J, Grygoryeva K, Lengyel J, Fárník M & Fedor J 2016 *Eur. Phys. J. D* **70**(4), 98.
Kočišek J, Papp P, Mach P, Vasilev Y V, Deinzer M L & Matejčík 2010 *J. Phys. Chem. A* **114**(4), 1677–1683.
Kočišek J, Pysanenko A, Fárník M & Fedor J 2016 *J. Phys. Chem. Lett.* **7**(17), 3401–3405.
Kunitsa A & Bravaya K 2016 *Phys. Chem. Chem. Phys.* **18**, 3454.
Lane A M & Thomas R G 1958 *Rev. Mod. Phys.* **30**, 257–353.
Lane N F 1980 *Rev. Mod. Phys.* **52**, 29–119.
Levesque P L, Michaud M & Sanche L 2005 *J. Chem. Phys.* **122**(9), 094701.
Li Z, Milosavljevic A, Carmichael I & Ptasinska S 2017 *submitted* .
Linert I & Zubek M 2006 *J. Phys. B* **39**(20), 4087.

Linert I & Zubek M 2015 *Chem. Phys. Lett.* **624**, 1.
Linert I & Zubek M 2016 *Eur. Phys. J. D* **70**(4), 74.
Maddern T M, Jamier V, Brunton J R, Brunger M J, Papamical C, Smith S V & Buckman S J 2016 *Int. J. Mass Spectrom.* **409**, 73 – 80.
Marangos J P 2016 *J. Phys. B* **49**(13), 132001.
Marinković B P, Vujćić V, Sushko G, Vudragović D, Marinković D B, Djordjević S, Ivanović S, Nešić M, Jevremović D, Solov'yov A V & Mason N J 2015 *Nucl. Instrum. Meth. B* **354**, 90 – 95.
Mauracher A, Denifl S, Aleem A, Wendt N, Zappa F, Cicman P, Probst M, Märk T D, Scheier P, Flosadóttir H D, Ingolfsson O & Illenberger E 2007 *Phys. Chem. Chem. Phys.* **9**, 5680–5685.
Mašín Z & Gorfinkiel J D 2011 *The Journal of Chemical Physics* **135**(14), 144308.
Mašín Z & Gorfinkiel J D 2014 *Eur. Phys. J. D* **68**(5), 1–8.
Mašín Z, Gorfinkiel J D, Jones D B, Bellm S M & Brunger M J 2012 *J. Chem. Phys.* **136**(14), 144310.
McAllister M, Smyth M, Gu B, Tribello G & Kohanoff J 2015 *J. Phys. Chem. Lett.* **6**(15), 3091–3097.
Minns R S & Kirrander A 2016 *Faraday Discuss.* **194**, 11–13.
Modelli A, Bolognesi P & Avaldi L 2011 *J. Phys. Chem. A* **115**(39), 10775–10782.
Modelli A & Burrow P D 1984 *Journal of Physical Chemistry* **88**, 3550.
Modelli A & Galasso V 2007 *J. Phys. Chem. A* **111**(32), 7787–7792.
Modelli A, Jones D & Distefano G 1982 *Chem. Phys. Lett.* **86**(4), 434 – 437.
Modelli A, Jones D & Pshenichnyuk S A 2013 *J. Chem. Phys.* **139**(18), 184305.
Modelli A & Pshenichnyuk S A 2013 *Phys. Chem. Chem. Phys.* **15**(5), 1588–1600.
Możejko P, Ptasińska-Denga E, Domaracka A & Szmytkowski C 2006 *Phys. Rev. A* **74**, 012708.
Muftakhov M V & Shchukin P V 2011*a* *Phys. Chem. Chem. Phys.* **13**, 4600–4606.
Muftakhov M V & Shchukin P V 2011*b* *Russian Chemical Bulletin* **60**(10), 1965–1976.
Muftakhov M V & Shchukin P V 2016 *Rapid Commun. Mass Spectrom.* **30**(24), 2577–2584.
Naaman R & Sanche L 2007 *Chem. Rev.* **107**(5), 1553–1579.
Nandi D, Prabhudesai V & Krishnakumar E 2006 *Rad. Phys. Chem.* **75**(12), 2151 – 2158.
Nandi D, Prabhudesai V S, Krishnakumar E & Chatterjee A 2005 *Rev. Sci. Instrum.* **76**(5), 053107.
Nenner I & Schulz G J 1975 *J. Chem. Phys.* **62**, 1747.
Neustetter M, Aysina J, daSilva F F & Denifl S 2015 *Angew. Chem., Int. Ed.* **54**(31), 9124–9126.
Neves R F C, Jones D B, Lopes M C A, Blanco F, García G, Ratnavelu K & Brunger M J 2015 *J. Chem. Phys.* **142**(19), 194305.
Neves R F C, Jones D B, Lopes M C A, Nixon K L, da Silva G B, Duque H V, de Oliveira E M, da Costa R F, do N. Varella M T, Bettega M H F, Lima M A P, Ratnavelu K, García G & Brunger M J 2015 *The Journal of Chemical Physics* **142**(10), 104305.
Nikjoo H, Emfietzoglou D, Liamsuwan T, Taleei R, Liljequist D & Uehara S 2016 *Rep. Prog. Phys.* **79**(11), 116601.
Nikjoo H, Taleei R, Liamsuwan T, Liljequist D & Emfietzoglou D 2016 *Rad. Phys. Chem.* **128**, 3 – 10.
Nunes F B, Bettega M H F & dAlmeida Sanchez S 2016 *J. Chem. Phys.* **145**(21), 214313.
Ómarsson B 2014 Promoting reaction channels in dissociative electron attachment through bond formation and rearrangement PhD thesis University of Iceland.
URL: *http://skemman.is/en/stream/get/1946/17817/41585/1/Thesis_BO.pdf*
Palihawadana P, Boadle R, Chiari L, Anderson E K, Machacek J R, Brunger M J, Buckman S J & Sullivan J P 2013 *Phys. Rev. A* **88**, 012717.
Palihawadana P, Sullivan J, Brunger M, Winstead C, McKoy V, García G, Blanco F & Buckman S 2011 *Phys. Rev. A* **84**, 062702.
Panosetti C, Baccarelli I, Sebastianelli F & Gianturco F A 2010 *Eur. Phys. J. D* **60**(1), 21–30.
Pimblott S M & LaVerne J A 2007 *Rad. Phys. Chem.* **76**(8-9), 1244 – 1247.
Prell J S, OBrien J T, Holm A I S, Leib R D, Donald W A & Williams E R 2008 *J. Am. Chem. Soc.* **130**(38), 12680–12689.
Pronschinske A, Pedevilla P, Murphy C J, Lewis E A, Lucci F R, Brown G, Pappas G, Michaelides A & Sykes E C H 2015 *Nat. Mater.* **14**(9), 904–907.

Pshenichnyuk S A & Modelli A 2012 *J. Chem. Phys.* **136**(23), 234307.
Pshenichnyuk S A & Modelli A 2013 *Phys. Chem. Chem. Phys.* **15**(23), 9125–9135.
Pshenichnyuk S A & Modelli A 2014 *J. Chem. Phys.* **140**(3), 034313.
Pshenichnyuk S A, Modelli A, Lazneva E F & Komolov A S 2016 *J. Phys. Chem. A* **120**(17), 2667–2676.
Ptasińska S, Alizadeh E, Sulzer P, Abouaf R, Mason N J, Märk T D & Scheier P 2008 *Int. J. Mass Spectrom.* **277**(13), 291 – 295.
Ptasinska S, Denifl S, Abedi A, Scheier P & Märk T D 2003 *Anal. Bioanal. Chem.* **377**(7), 1115–1119.
Ptasińska S, Denifl S, Candori P, Matejčík S, Scheier P & Märk T 2005 *Chem. Phys. Lett.* **403**(13), 107 – 112.
Ptasinska S, Denifl S, Gohlke S, Scheier P, Illenberger E & Märk T D 2006 *Angew. Chem., Int. Ed.* **45**(12), 1893–1896.
Ptasinska S, Denifl S, Grill V, Illenberger T D M E & Scheier P 2005 *Phys. Rev. Lett.* **95**(9), 093201.
Ptasinska S, Denifl S, Scheier P, Illenberger E & Märk T 2005 **44**(42), 6941–6943.
Ptasinska S, Denifl S, Scheier P & Märk T 2004 *J. Chem. Phys.* **120**, 8505–8511.
Puschnigg B, Huber S E, Probst M, Tanzer K, Vizcaino V, Ferreira da Silva F, Scheier P, Limão-Vieira P & Denifl S 2013 *Phys. Chem. Chem. Phys.* **15**, 3834–3840.
Puschnigg B, Huber S E, Scheier P, Probst M & Denifl S 2014 *Eur. Phys. J. D.* **68**(5), 119.
Rackwitz J, Kopyra J, Dbkowska I, Ebel K, Rankovi M L, Milosavljevi A R & Bald I 2016 *Angew. Chem., Int. Ed.* **55**(35), 10248–10252.
Read F H & Channing J M 1996 *Rev. Sci. Instrum.* **67**(6), 2372–2377.
Regeta K & Allan M 2015 *Phys. Rev. A* **91**, 012707.
Regeta K, Allan M, Mašín Z & Gorfinkiel J D 2016 *J. Chem. Phys.* **144**(2), 024302.
Regeta K, Allan M, Winstead C, McKoy V, Mašín Z & Gorfinkiel J D 2016 *J. Chem. Phys.* **144**(2), 024301.
Rescigno T N, Trevisan C S & Orel A E 2006 *Phys. Rev. Lett.* **96**, 213201.
Ridenti M A, Filho J A, Brunger M J, da Costa R F, Varella M T d N, Bettega M H & Lima M A 2016 *Eur. Phys. J. D* **70**(8), 161.
Rudek B, Bennett D, Bug M U, Wang M, Baek W Y, Buhr T, Hilgers G, Champion C & Rabus H 2016 *J. Chem. Phys.* **145**(10), 104301.
Ryszka M, Sieradzka A, Pandey R, Dampc M, Man Z, Eden S & Gorfinkiel J D 2015 *J. Phys.: Conf. Ser.* **635**(7), 072052.
Samukawa S, Hori M, Rauf S, Tachibana K, Bruggeman P, Kroesen G, Whitehead J C, Murphy A B, Gutsol A F, Starikovskaia S, Kortshagen U, Boeuf J P, Sommerer T J, Kushner M J, Czarnetzki U & Mason N 2012 *J. Phys. D: Appl. Phys.* **45**(25), 253001.
Sanche L 2005 *Eur. Phys. J. D* **35**(2), 367–390.
Sanche L 2015 *Nat. Mater.* **14**(9), 861–863.
Sanche L 2016 *Rwd. Phys. Chem.* **128**, 36 – 43.
Sanna N, Baccarelli I & Morelli G 2009 *Computer Phys. Comm.* **180**(12), 2550–2562.
Sanz A, Fuss M, Blanco F, Mašín Z, Gorfinkiel J D, Carelli F, Sebastianelli F, Gianturco F & García G 2014 *Applied Radiation and Isotopes* **83, Part B**(0), 57 – 67.
Sanz A G, Fuss M C, Blanco F, Mašín Z, Gorfinkiel J D, McEachran R P, Brunger M J & García G 2013 *Phys. Rev. A* **88**, 062704.
Scheer A M, Aflatooni K, Gallup G A & Burrow P D 2004 *Phys. Rev. Lett.* **92**(6), 068102.
Scheer A M, Aflatooni K, Gallup G A & Burrow P D 2014 *J. Phys. Chem. A* **118**(35), 7242–7248.
Scheer A, Mozejko P, Gallup G & Burrow P 2007 *J. Chem. Phys.* **126**(17), 174301.
Schulz G J 1973*a* *Rev. Mod. Phys.* **45**(3), 378.
Schulz G J 1973*b* *Rev. Mod. Phys.* **45**(3), 423.
Shchukin P V, Muftakhov M V, Morr J, Deinzer M L & Vasilev Y V 2010 *J. Chem. Phys.* **132**(23), 234306.
Shchukin P V, Muftakhov M V & Pogulay A V 2012 *Rapid Commun. Mass Spectrom.* **26**(7), 828–834.
Sieradzka A & Gorfinkiel J D 2017 *J. Chem. Phys.* (under review).

Silva F F, Matias C, Almeida D, García G, Ingólfsson O, Flosadóttir H D, Ómarsson B, Ptasinska S, Puschnigg B, Scheier P, Limão-Vieira P & Denifl S 2013 *Journal of The American Society for Mass Spectrometry* **24**(11), 1787–1797.

Slaughter D S, Belkacem A, McCurdy C W, Rescigno T N & Haxton D J 2016 *J. Phys. B* **49**(22), 222001.

Smyth M, Kohanoff J & Fabrikant I I 2014 *J. Chem. Phys.* **140**(18), 184313.

Sobczyk M, Anusiewicz I, Berdys-Kochanska J, Sawicka A, Skurski P & Simons J 2005 *J. Phys. Chem. A* **109**(1), 250–258.

Sulzer P, Alizadeh E, Mauracher A, Märk T D & Scheier P 2008 *Int. J. Mass Spectrom.* **277**(13), 274 – 278.

Surdutovich E, Setzler G, Kauppila W E, Rehse S J & Stein T S 2008 *Phys. Rev. A* **77**, 054701.

Surko C M, Gribakin G F & Buckman S J 2005 *J. Phys. B* **38**(6), R57.

Takatsuka K & McKoy V 1984 *Phys. Rev. A* **30**, 1734–1740.

Tanzer K, Feketeová L, Puschnigg B, Scheier P, Illenberger E & Denifl S 2014 *Angew. Chem., Int. Ed.* **53**(45), 12240–12243.

Tanzer K, Feketeová L, Puschnigg B, Scheier P, Illenberger E & Denifl S 2015 *J. Phys. Chem. A* **119**(25), 6668–6675.

Tanzer K, Pelc A, Huber S, Śmiałek M, Scheier P, Probst M & Denifl S 2014 *Int. J. Mass Spectrom.* **365-366**, 152 – 156.

Tashiro M 2008 *J. Chem. Phys.* **129**, 164308.

Tennyson J 2010 *Phys. Rep.* **491**, 29–76.

Tonzani S & Greene C H 2006 *J. Chem. Phys.* **124**, 054312.

Trevisan C S, Orel A E & Rescigno T N 2006 *J. Phys. B: At. Mol. Opt. Phys.* **39**, L255–L260.

Vasil'ev Y V, Figard B J, Morré J & Deinzer M L 2009 *J. Chem. Phys.* **131**(4), 044317.

Vasil'ev Y V, Figard B J, Voinov V G, Barofsky D F & Deinzer M L 2006 *J. Am. Chem. Soc.* **128**(16), 5506–5515.

Vasilev Y V, Figard B J, Barofsky D F & Deinzer M L 2007 *Int. J. Mass Spectrom.* **268**(23), 106 – 121.

Vizcaino V, Bartl P, Gschliesser D, Huber S E, Probst M, Märk T D, Scheier P & Denifl S 2011 *ChemPhysChem* **12**(7), 1272–1279.

Vizcaino V, Puschnigg B, Huber S E, Probst M, Fabrikant I I, Gallup G A, Illenberger E, Scheier P & Denifl S 2012 *New J. Phys.* **14**(4), 043017.

Wang C R, Nguyen J & Lu Q B 2009 *J. Am. Chem. Soc.* **131**(32), 11320–11322.

Wang Y F, Tian S X & Yang J 2011 *Phys. Chem. Chem. Phys.* **13**(34), 15597–15602.

Weinberger N, Ralser S, Renzler M, Harnisch M, Kaiser A, Denifl S, Boehme D K & Scheier P 2016 *Eur. J. Phys. D* **70**(4), 91.

Winstead C & McKoy V 1996 *in* Bederson, B and Walther, H, ed., 'Adv. At. Mol. Opt. Phys.' Vol. 36 Elsevier pp. 183–219.

Winstead C & McKoy V 2006*a* *J. Chem. Phys.* **125**(7), 074302.

Winstead C & McKoy V 2006*b* *J. Chem. Phys.* **125**(24), 244302.

Winstead C & McKoy V 2006*c* *J. Chem. Phys.* **125**(17), 174304–8.

Winstead C & McKoy V 2007 *Phys. Rev. Lett.* **98**, 113201.

Winstead C & McKoy V 2008 *Rad. Phys. Chem.* **77**(1012), 1258 – 1264.

Winstead C, McKoy V & dAlmeida Sanchez S 2007 *J. Chem. Phys.* **127**(8), 085105.

Yoon J S, Song M Y, Kwon D C, Choi H, Kim C G & Kumar V 2014 *Phys. Rep.* **543**(4), 199 – 244.

Zecca A, Perazzolli C & Brunger M 2005 *J. Phys. B: At. Mol. Opt. Phys.* **38**(13), 2079–2086.

Zubek M, Dampc M, Linert I & Neumann T 2011 *J. Chem. Phys.* **135**(13), 134317.

Zubek M, Gulley N, King G C & Read F H 1996 *J. Phy. B* **29**(6), L239.